REPORT DOCUMENTATION PAGE

Form Approved
OMB No. 0704-0188

1. REPORT DATE *(DD-MM-YYYY)*	**2. REPORT TYPE**	**3. DATES COVERED** *(From - To)*
13-04-2012	Thesis	

4. TITLE AND SUBTITLE

Impact of Liquid Propellant Properties on Small Energy Conversion Device Dimensions

5a. CONTRACT NUMBER

5b. GRANT NUMBER

5c. PROGRAM ELEMENT NUMBER

6. AUTHOR(S)
A. Zuttarelli and T. Fox

5d. PROJECT NUMBER

5f. WORK UNIT NUMBER
48471029

7. PERFORMING ORGANIZATION NAME(S) AND ADDRESS(ES)

Air Force Research Laboratory (AFMC)
AFRL/RZSS
1 Ara Drive
Edwards AFB CA 93524-7013

8. PERFORMING ORGANIZATION REPORT NUMBER

9. SPONSORING / MONITORING AGENCY NAME(S) AND ADDRESS(ES)

Air Force Research Laboratory (AFMC)
AFRL/RZS
5 Pollux Drive
Edwards AFB CA 93524-7048

10. SPONSOR/MONITOR'S ACRONYM(S)

11. SPONSOR/MONITOR'S NUMBER(S)
AFRL-RZ-ED-TP-2012-126

12. DISTRIBUTION / AVAILABILITY STATEMENT
Distribution A: Approved for public release; distribution unlimited PA# 12256

13. SUPPLEMENTARY NOTES
Thesis presentation for California State University Northridge, Northridge, CA, 11 May 2012.

14. ABSTRACT
A study has been made of how the physical properties of the liquid propellants hydrazine and hydrogen peroxide influence energy conversion device dimensions across multiple operating configurations. The energy conversion device was a staged rocket thruster comprised of a first stage where propellant is decomposed to create a high temperature, low velocity environment and a second stage downstream where propellant is injected and exothermically decomposed. The operating configurations varied chamber pressure, propellant flow rate ratio of first stage to second stage, and ratio of propellant feed pressure to chamber pressure within the thruster. Chamber pressures of 125, 250, and 500 psi; flow rate ratios of 1:3, 1:4, and 1:5; and feed to chamber pressure ratios of 1.25:1 and 1.75:1 were considered. The study utilizes relationships that were empirically derived to estimate droplet sizes as a function of the propellant physical properties and various related operating conditions. As the chamber pressure and feed to chamber pressure ratio increased, the chamber dimensions decreased. As the flow rate ratio decreased, the chamber length increased. Relative to the primary reference, Ryan1, empirical data values achieved in the instant study were consistently 30-50% low. Contributing to the disagreement, was use of injector orifice diameters below those of the reference which would drive increased injection velocity values and drive the results lower.

15. SUBJECT TERMS

16. SECURITY CLASSIFICATION OF:			**17. LIMITATION OF ABSTRACT**	**18. NUMBER OF PAGES**	**19a. NAME OF RESPONSIBLE PERSON**
					Anthony P. Zuttarelli
a. REPORT	**b. ABSTRACT**	**c. THIS PAGE**			**19b. TELEPHONE NUMBER** *(include area code)*
Unclassified	**Unclassified**	**Unclassified**	SAR	69	N/A

CALIFORNIA STATE UNIVERSITY, NORTHRIDGE

Impact of Liquid Propellant Properties on Small Energy Conversion Device Dimensions

A thesis submitted in partial fulfillment of the requirements

For the degree of Master of Science in Engineering

By

Anthony Zuttarelli

May 2012

Signature Page

The thesis of Anthony P. Zuttarelli is approved:

_____	_____
William Hargus, Ph. D.	Date
_____	_____
Professor Sidney Schwartz	Date
_____	_____
Professor Timothy Fox, Chair	Date

California State University, Northridge

Table of Contents

List of Tables

List of Figures

Abstract

A study has been made of how the physical properties of the liquid propellants hydrazine and hydrogen peroxide influence energy conversion device dimensions across multiple operating configurations. The energy conversion device was a staged rocket thruster comprised of a first stage where propellant is decomposed to create a high temperature, low velocity environment and a second stage downstream where propellant is injected and exothermically decomposed. The operating configurations varied chamber pressure, propellant flow rate ratio of first stage to second stage, and ratio of propellant feed pressure to chamber pressure within the thruster. Chamber pressures of 125, 250, and 500 psi; flow rate ratios of 1:3, 1:4, and 1:5; and feed to chamber pressure ratios of 1.25:1 and 1.75:1 were considered. The study utilizes relationships that were empirically derived to estimate droplet sizes as a function of the propellant physical properties and various related operating conditions. As the chamber pressure and feed to chamber pressure ratio increased, the chamber dimensions decreased. As the flow rate ratio decreased, the chamber length increased. Relative to the primary reference, Ryan[1], empirical data values achieved in the instant study were consistently 30-50% low. Contributing to the disagreement, was use of injector orifice diameters below those of the reference which would drive increased injection velocity values and drive the results lower.

Section 1: Introduction

Background

With attention to alternative and less environmentally impactful energy sources to support the established transportation and power infrastructure of the world's growing needs, the impact of even a small change to present day formulations of the fuels and propellants manufacture, synthesis and waste products, and applicability to energy conversion equipment already in widespread use must be considered. Focusing from the wide scope of these considerations to one area that is highly mass, power, and volume constrained-the aerospace satellite industry, there is particular interest in expansion and life extension of current day thruster technologies that reduce the "foot print" of on board propulsive systems to increase power, mass, and volume available to the payload. The payoff of a more compact, less spacecraft power expensive propulsion system that can cover a wider range of operation can show immediate benefits to payload capacity. The focus of this engineering study is to consider an alternative thruster concept and the impact on the volumetric footprint of the thruster based upon the properties of the liquid propellants commonly in use today and provide for first iteration estimates of propellant formulation change impact to state of the art energy conversion hardware. The algorithms are derived from previous empirical studies performed and could be applied to other liquid propellant formulations. The instant study considers state of the art monopropellant hydrazine, N_2H_4, and hydrogen peroxide, H_2O_2, for comparison of impact of properties as the liquid propellants. Development of energy conversion devices such as liquid chemical thrusters incurs great expense, especially in the early

phases of isolating configurations that will cover a desired operational range. As a minimum, being able to leverage from existing proven designs decreases developmental effort and supports speeding transition to use. From this engineering study a design tool results with capability to provide rough, first approximation of developmental hardware as functions of the liquid properties and design operating parameters. With a reasonable first guess of what the range of dimensions the hardware will be, some non-recurring costs can be avoided. Also, by allowing for various operational inputs such as the chamber temperature and pressure, one can include considerations of duty cycles required by mission.

Configuration

For the purpose of the instant study, a thrust level of 5 pounds force has been chosen. The aspect of configuration that this operational parameter sets is ultimately the flow rate of propellant, which will then influence the overall dimensions of the device. The configuration of the thruster could be considered bimodal in the regard that with appropriate control of propellants, two levels of thrust from the same thruster body can be provided. Typically, spacecraft will carry both low force thrusters for use in attitude adjustments and increased force thrusters for trajectory adjustments. The configuration, shown in FIGURE 1, comprises a de Laval type converging-diverging type nozzle that is commonly used in rocket thrusters. In this configuration there are two feeds of propellant into the device, an initial feed into an ignition or decomposition inducing device to transition the liquid propellant into a high temperature gas and a second feed downstream of the exit of the decomposition device through multiple, impinging injectors.

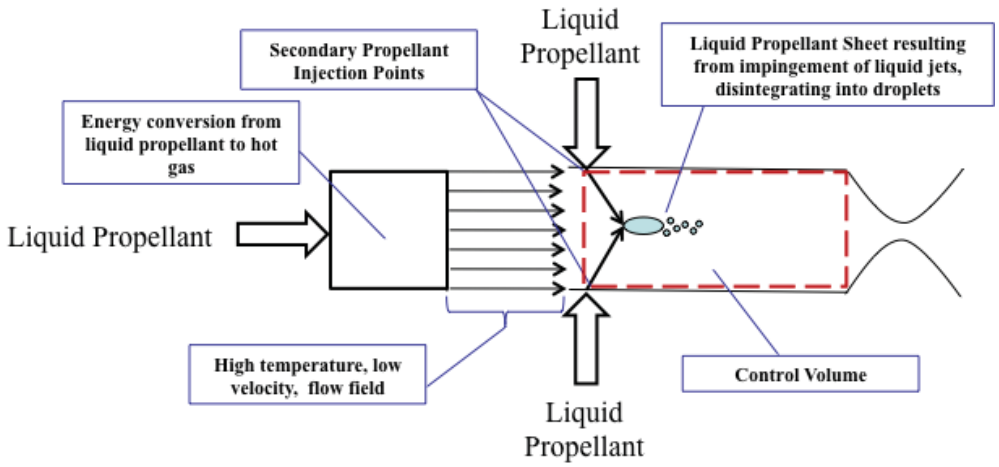

FIGURE 1. Thruster configuration diagram

The initial feed in this study is construed to be flowing into a catalytic reactor, the common decomposition device for the propellants being considered. Downstream at the second point of injection are two opposed injection orifice that will result in the two liquid propellant streams impinging and atomizing. The droplets resulting from the atomization are subjected to the high temperature, low velocity flow resulting from the previously decomposed propellant and then also transition into a high temperature gas. The sum total of high temperature gas then exits the throat. The area of FIGURE 1 bordered by the red dashed line constitutes the area of interest where calculations will be focused, based upon propellant physical properties to derive chamber dimensions. FIGURE 2 shows the area of particular interest noted in regards to FIGURE 1, with an additional dashed orange perimeter defining the area of interest in regards to estimates based upon established empirical relationships to determine distance required for impingement and atomization to occur.

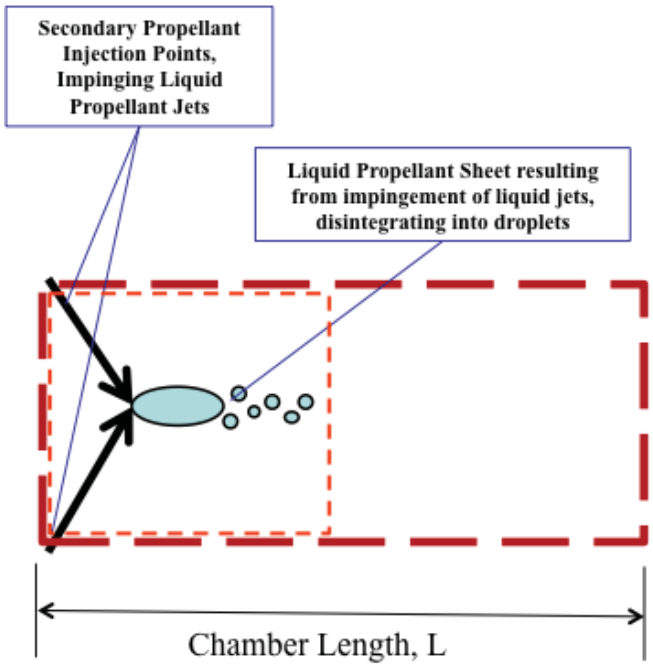

FIGURE 2. Control volume under consideration

Physical Process

Multiple physical processes are involved in nominal thruster operation, encompassing the injection of a liquid propellant and its exothermic conversion to high temperature, expanded gas. The initial step of injection will track the physical state of the liquid propellant via the terms of viscosity, density, surface tension, and calculated chamber temperature. These properties will, in addition to the injection velocity and the injector configuration, control the atomization of the liquid propellant. The liquid propellants of the instant model will be injected into a high-temperature, low velocity, flowing gas field where heat transfer will take place via convection to impart heat to the atomized propellants and increase their temperature to flash point. TABLE 1 summarizes the liquid propellant properties of interest that impact atomization.

Liquid Property	Symbol	Unit	Definition
Coefficient of Viscosity, Dynamic	μ_L	kg/(m-s)	Constant of proportionality of applied shear to the velocity gradient of common linear fluids[3]
Coefficient of Viscosity, Kinematic	ν_L	m^2/s	Ratio of dynamic viscosity coefficient to density[3]
Density	ρ_L	kg/m^3	Mass per unit volume
Surface Tension	σ_L	kg/s^2	Property that resists expansion of liquid surface area[5]

TABLE 1. Relevant Physical Liquid Propellant Properties

The resulting size of droplets within the atomized dispersion will control the residence time required for the droplets to absorb enough heat from the high temperature environment to transition to vapor. The vapor state will be considered the point at which exothermic reaction ensues. The distance traveled will set the chamber length. The chamber length will be a function of the liquid physical properties, injection angle and velocity, and thermal environment to which the atomized field is exposed. A visualization of this general concept as presented by one of the primary references, Ryan[1], is shown in FIGURE 3, where two impinging liquid jets form a liquid sheet which then breaks down into ligaments and then drops.

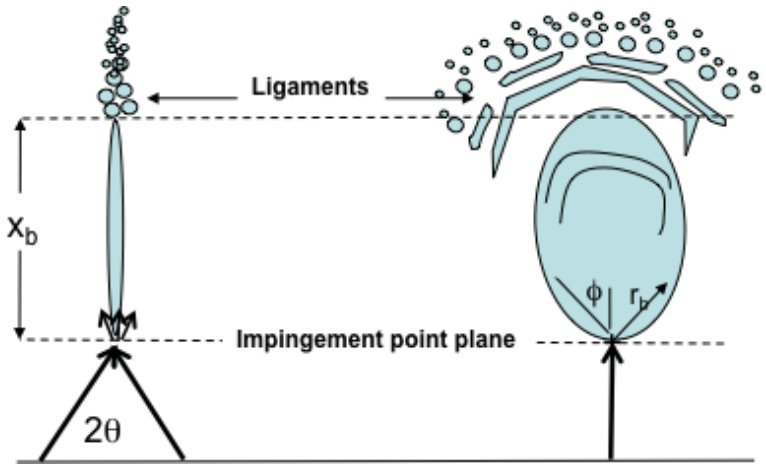

FIGURE 3. Visualization of the atomization process (figure 1 from Ryan[1])of two impinged streams of liquid, left hand view is 90° to the right hand view

FIGURE 3 also shows some relevant nomenclature, which will be referred to frequently through out this study. The break up radius, r_b, of the impingement sheet for a given angular displacement, ϕ, from the centerline of the impingement sheet is shown, where the origin is set at the point of impingement. The impingement half angle, θ, is shown and plays a significant role throughout the calculations. The centerline impingement sheet distance, X_b, is shown which indicates the point where r_b at an angular displacement, ϕ, of 0^o, lies and indicates where ligament separation will begin on the liquid sheet. Throughout the remainder of this paper, reference will only be made r_b. FIGURE 4, 5, and 6 are photos of impingement sheets under turbulent and laminar conditions showing length scales associated therewith taken from Ryan.

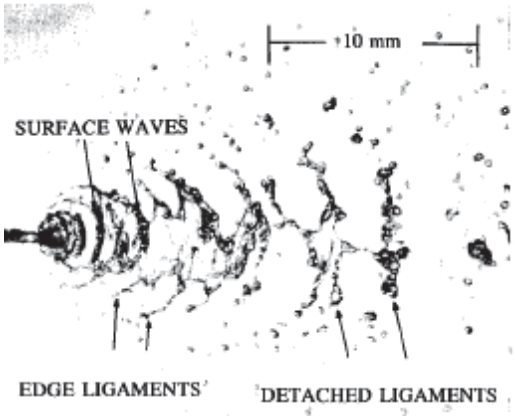

FIGURE 4. Typical spray formed by turbulent impinging jets with the elements of an impingement sheet degrading into ligaments and then drops shown(figure 9 from Ryan)

FIGURE 4 is an impingement sheet formed of turbulent impinging jets with the various elements of degradation noted. Here it can be seen, a liquid sheet forms, then degrades to ligaments, which then degrade into drops. FIGURE 5 shows a similar photo of a turbulent sheet, which can be contrasted with that in FIGURE 6 which is a laminar sheet.

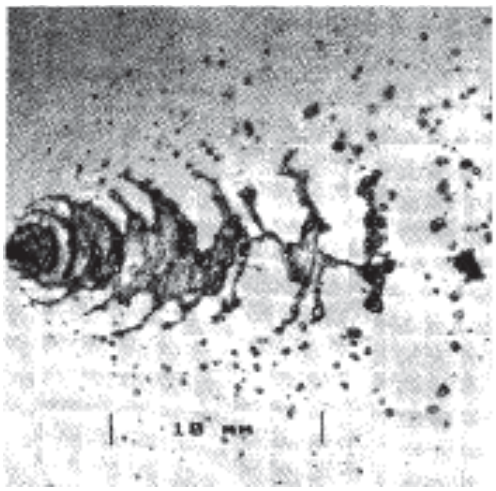

FIGURE 5. Low jet velocity (6.4 m/s) turbulent impingement sheet photo (figure 3a from Ryan)

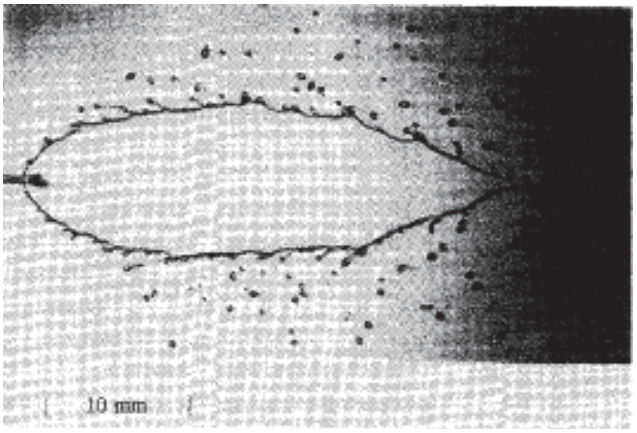

FIGURE 6. Low jet velocity (7.1 m/s) laminar impingement sheet photo (figure 4a from Ryan)

Contrasting FIGURE 5 and 6, in the interest of compactness it would appear that turbulent flow is desired since the degradation into drops occurs more quickly. The basis of Ryan's theoretical determination of drop size relies upon sheet break up due to aerodynamic forces and does not account for any disturbance introduced to the sheet from shock waves induced from the impingement itself. It will become evident in the results that this aspect needs to be accounted for to have a complete model to describe

impingement sheet length. Recall, in the instant study this is the secondary or downstream injection of propellant and thus the atomization occurs in a high temperature, low velocity gas environment. Empirical relations are taken from Ryan that estimate the resultant sheet length and drop size. Contributors to the total chamber length calculation will be the distance from the injector orifice to the impingement point, the centerline distance of the resultant liquid sheet, and the distance required for the resultant drops to transition to the vapor state within the high temperature gas, low velocity gas flow from the catalytic reactor.

Propellants

The liquid propellants in the instant investigation, hydrazine (N_2H_4) and hydrogen peroxide (H_2O_2) are considered earth storable. Earth storable propellants typically do not require extensive environmental controls beyond material compatibility and pressure relief for conditions well beyond room temperature. These propellants have been in common use for the last 40+ years, their properties well documented, and with many thruster configurations developed. The properties primarily of interest to this study are shown in TABLE 2.

Propellant	Liquid Property	Symbol	Value Range	Units	Value Constraints
N_2H_4	Coefficient of Viscosity, Dynamic	μ_L	**9.736×10^{-4}**	kg/(m-s)	**20°C**
	Coefficient of Viscosity, Kinematic	ν_L	**9.654×10^{-7}**	m^2/s	**20°C**
	Density	ρ_L	**1.009×10^{3}**	kg/m^3	**20°C**
	Surface Tension	σ_L	**6.850×10^{-4}**	kg/s^2	**20°C**
H_2O_2	Coefficient of Viscosity, Dynamic	μ_L	**1.250×10^{-3}**	kg/(m-s)	**20°C**
	Coefficient of Viscosity, Kinematic	ν_L	**8.621×10^{-7}**	m^2/s	**20°C**
	Density	ρ_L	**1.450×10^{3}**	kg/m^3	**20°C**
	Surface Tension	σ_L	**8.013×10^{-4}**	kg/s^2	**20°C**

TABLE 2. Relevant Physical Properties of Propellants

Properties that impact liquid behavior at injection including feed velocity, liquid propellant feed temperature and injector configuration properties will be considered. The extent of the liquid propellant temperature impact resides solely in the values of the viscosity, density, and surface tension. As shown by the previous FIGURES 1 and 2, the propellants will be injected into the high temperature gas created by the catalytic decomposition of a small amount of that same propellant upstream. Keeping track of the products of decomposition is critical since in the succeeding empirical relationships applied, the density of the gas of the environment the propellants are injected into are required to successfully calculate evolved drop size from the impingement and atomization of the propellants.

Propellants-Hydrazine (N_2H_4)

The first propellant of interest is hydrazine, N_2H_4. The following expression, taken from Schmidt[2], for the catalytic decomposition path for hydrazine is ideally as shown in Reaction 1 to produce high temperature nitrogen and hydrogen, and is a function of the ammonia produced.

$$3\ N_2H_4 \rightarrow 4\ (1\text{-}X)NH_3 + (1+2X)N_2 + 6XH_2$$

Reaction 1. Hydrazine decomposition as a function of Ammonia dissociation

Where ammonia dissociation is expressed with the X term and is proportional to the ratio of bedloading, G; dwell time, t; pressure, p; and r is an empirically derived constant fitted to give best correlation to data. More directly written, the relationship for ammonia dissociation, X, is defined in EQUATION 1.

$$[1] \qquad X \sim G^{0.71} t/p^{r}$$

The scaling relationship set forth by Schmidt[2] for the amount of ammonia dissociation provides insight for specific operating conditions and configurations. This relationship would certainly provide a superior insight into the ammonia dissociation related to hydrazine decomposition. In the absence of the data set required to derive the power term r, a general guidance is provided by Brown[3] stating that ammonia dissociation is generally kept below 50% in hydrazine engines. Where the ammonia dissociation is 50%, the following decomposition path is applied for hydrazine in Reaction 2.

$$3\ N_2H_4 \rightarrow 2NH_3 + 2N_2 + 3H_2$$

Reaction 2. Hydrazine decomposition at 50% Ammonia dissociation

The resultant temperature and specific impulse, I_{sp}, variations due to the amount of ammonia dissociation will have effect on the algorithms presented later. Specifically, the

temperature will impact the gas density of the environment where the secondary injection takes place as well as the time required for the droplets to reach their flame temperature. The I_{sp} will influence the flow rates at both the initial and secondary injection points, and thus in particular the flow velocity at the secondary injection point will influence the size of droplets produced from the atomization. An additional influence on the I_{sp} is nozzle expansion ratio, ε, and chamber pressure, P_c. To capture a relative indication of these impacts, values over range of conditions are captured in TABLE 3 with accompanying plot in FIGURE 3.

Propellant	P_c (psia)	T_c (K)	% NH_3 dissociation	Condition	I_{sp} throat	ε	I_{sp} Nozzle Exit
N_2H_4	125	874.6	100	SL	90.0	1.9	152.4
	250	880.8	100	SL	89.8	3.0	170.2
	500	891.5	100	SL	89.7	5.0	185.4
	125	874.6	100	Vac	156.4	1.9	179.7
	250	880.8	100	Vac	156.9	3.0	192.1
	500	891.5	100	Vac	157.7	5.0	203.7
	125	872.4	100	SL	89.9	50.0	220.8
	250	878.7	100	SL	89.8	50.0	222.5
	500	889.6	100	SL	89.9	50.0	222.5
	1000	906.5	100	SL	90.1	50.0	226.3
	125	872.4	100	Vac	156.2	50.0	230.6
	250	878.7	100	Vac	156.7	50.0	232.3
	500	889.6	100	Vac	157.5	50.0	234.2
	1000	906.5	100	Vac	158.6	50.0	236.2
	1000	860.0	100	Vac	---	50.0	212.0
	1000	1320.0	40	Vac	---	50.0	248.0
	1000	1500.0	20	Vac	---	50.0	258.0

TABLE 3. Hydrazine calculated I_{sp} values under varying conditions

Of note, the initial set of I_{sp} values are based upon expansion ratios optimized for atmospheric operation, where as the latter values are optimized with an expansion ratio of 50:1. With the exception of the last 3 values, derived from plots in Schmidt[2], ammonia dissociation is taken to be complete which impacts the chamber temperature, T_c, and the I_{sp}. The resulting reaction for an ammonia dissociation of 100% is in Reaction 3.

$$3\ N_2H_4 \rightarrow 3N_2 + 6H_2$$

Reaction 3. Hydrazine decomposition at 100% Ammonia dissociation

The difference in values is more easily identified in FIGURE 7. In this figure it is clearly seen how the endothermic process of ammonia dissociation impacts the overall calculated specific impulse, as well as the expansion ratio.

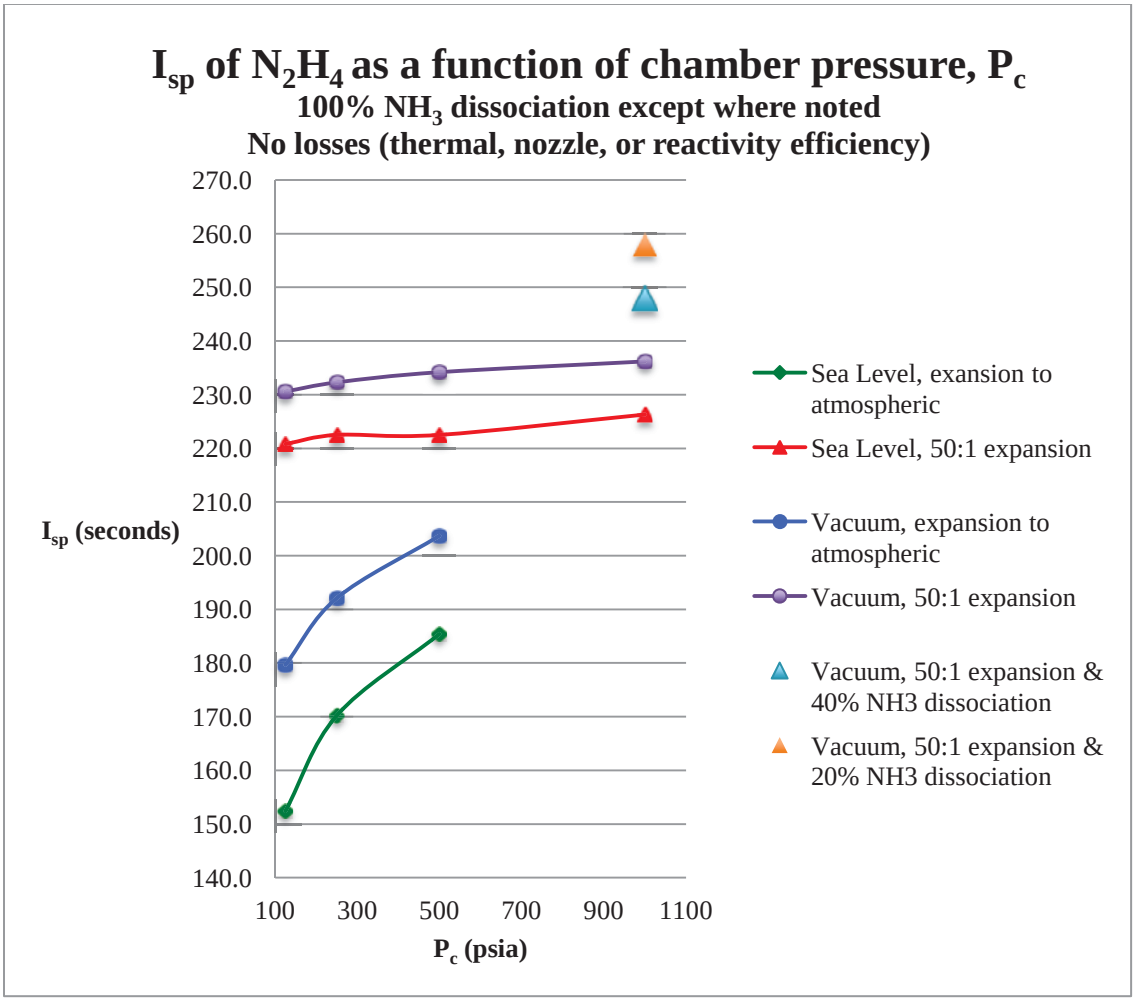

FIGURE 7. Hydrazine specific impulse as a function of chamber pressure showing the impact of expansion ratio and ammonia dissociation.

The values for I_{sp} and T_c are noticeably lower for complete ammonia dissociation than when it is held below 50% as noted by Brown[3]. For the purpose of this study, median

values were chosen at complete, or 100%, ammonia dissociation at the vacuum condition at an expansion ratio of 50:1.

Propellants-Hydrogen Peroxide (H_2O_2)

For the purpose of breadth and insight, Hydrogen peroxide, H_2O_2, at a 100% concentration is the other propellant of interest in this study. The decomposition path of hydrogen peroxide can theoretically be 10 to 20 reactions, however, per *The Hydrogen Peroxide Handbook*[4], the following reaction path is an effective result of these intermediate steps in the decomposition. Reaction 3 shows the cumulative reaction path that will be used for this study.

$$2\ H_2O_2 \rightarrow 2\ H_2O + O_2$$

Reaction 4. Hydrogen Peroxide decomposition reaction

TABLE 4 below shows a range of calculated values for the specific impulse at the same expansion ratios and chamber pressures as used for hydrazine above. The values for specific impulse are plotted in FIGURE 5. As with hydrazine, the decomposition of hydrogen peroxide does contain an endothermic quantity driven by its concentration. Reaction 4 above presumes a concentration of 100%, i.e. no dilution with water. The impact of concentration on the specific impulse and chamber temperatures calculated is substantial.

Propellant	P_c (psia)	T_c (K)	%H_2O	Condition	I_{sp} throat	ε	I_{sp} Nozzle Exit
H_2O_2	125	1274.8	0	SL	73.6	1.9	129.7
	250	1274.9	0	SL	73.6	3.0	144.2
	500	1274.8	0	SL	73.6	4.6	155.5
	125	1274.2	0	SL	73.7	50.0	185.4
	250	1274.2	0	SL	73.7	50.0	185.3
	500	1274.2	0	SL	73.7	50.0	185.2
	1000	1274.2	0	SL	73.7	50.0	185.1
	125	1274.8	0	Vac	132.2	1.9	153.5
	250	1274.9	0	Vac	132.2	3.0	162.5
	500	1274.8	0	Vac	132.2	4.6	169.9
	125	1274.2	0	Vac	132.2	50.0	190.9
	250	1274.2	0	Vac	132.2	50.0	191.0
	500	1274.2	0	Vac	132.2	50.0	191.1
	1000	1274.2	0	Vac	132.2	50.0	191.2
	125	1224.9	2	SL	72.5	50.0	181.7
	250	1224.9	2	SL	72.5	50.0	181.6
	500	1224.9	2	SL	72.5	50.0	181.6
	1000	1224.9	2	SL	72.5	50.0	181.6
	125	1224.9	2	Vac	129.9	50.0	187.3
	250	1224.9	2	Vac	129.9	50.0	187.4
	500	1224.9	2	Vac	129.9	50.0	187.6
	1000	1224.9	2	Vac	129.9	50.0	187.8
	125	1151.3	5	SL	70.6	50.0	176.1
	250	1151.3	5	SL	70.6	50.0	176.1
	500	1151.3	5	SL	70.6	50.0	176.1
	1000	1151.3	5	SL	70.6	50.0	176.2
	125	1151.3	5	Vac	126.3	50.0	181.9
	250	1151.3	5	Vac	126.3	50.0	182.1
	500	1151.3	5	Vac	126.3	50.0	182.3
	1000	1151.3	5	Vac	126.3	50.0	182.6
	125	1028.8	10	SL	67.3	50.0	166.7
	250	1028.8	10	SL	67.3	50.0	166.8
	500	1028.8	10	SL	67.3	50.0	167.0
	1000	1028.8	10	SL	67.3	50.0	167.2
	125	1028.8	10	Vac	119.9	50.0	172.8
	250	1028.8	10	Vac	199.9	50.0	173.1
	500	1028.8	10	Vac	119.9	50.0	173.4
	1000	1028.8	10	Vac	119.9	50.0	173.8

TABLE 4. Hydrogen peroxide calculated I_{sp} values under varying conditions

As was done with hydrazine, one particular specific impulse value was chosen for comparative analysis. In both cases, the calculated values that were used did not account for the losses that are typical within a thruster due to combustion or decomposition inefficiency, thermal losses to the thruster itself, and nozzle efficiency.

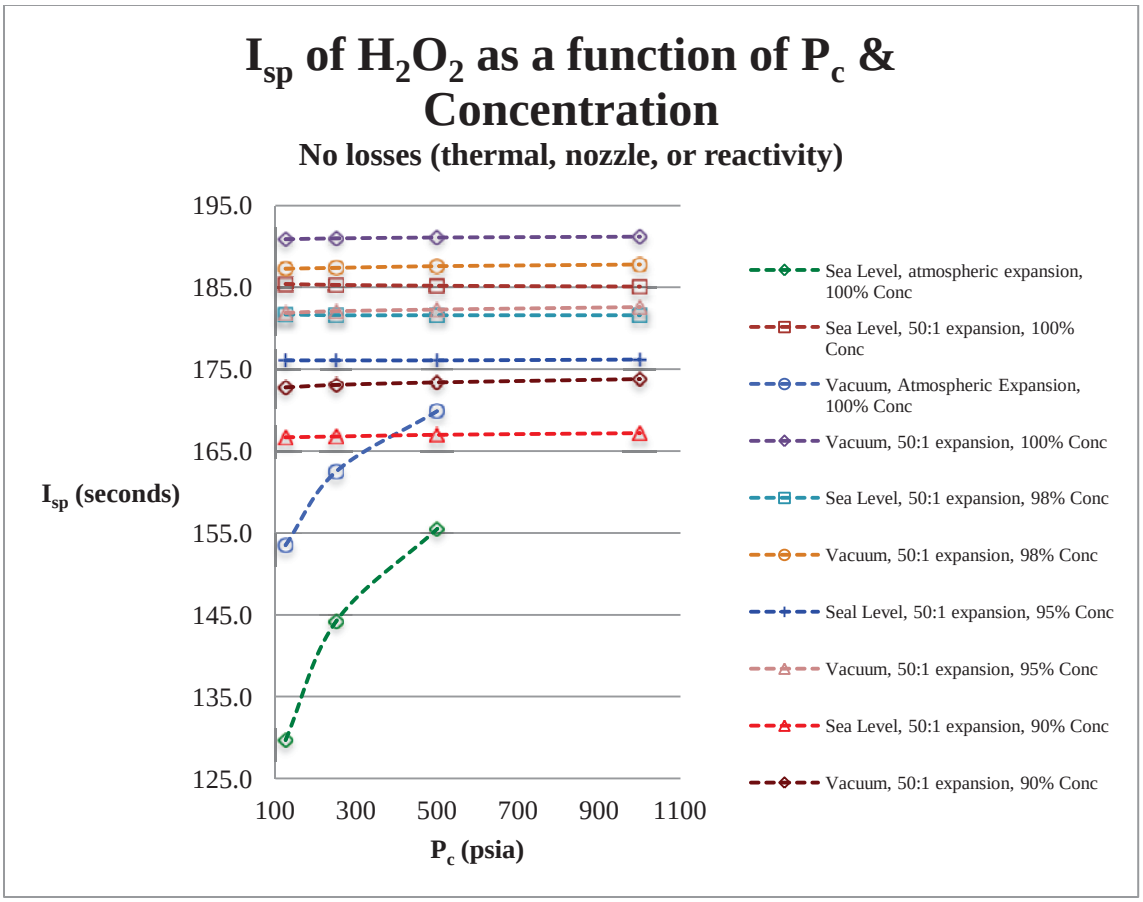

FIGURE 8. Hydrogen peroxide specific impulse as a function of chamber pressure showing the impact of expansion ratio and concentration.

As with the plot of hydrazine values shown in FIGURE 7, it is noticeable in FIGURE 8 how the chamber pressure is somewhat influential as well with hydrogen peroxide when expansion is optimized for sea level. The sensitivity of the specific impulse is removed when values are calculated at a set expansion ratio or vacuum conditions. Values chosen for the comparative analysis were at a concentration of 100%, vacuum, and fixed expansion ratio of 50:1. This choice minimizes the variance imposed upon the analysis to allow better visibility of the impact of propellant physical properties on chamber size.

Investigation Constraints and Presumptions

Weber and Reynolds Number

The impingement sheet and eventual drop size relations that underlie this study are provided by the empirical studies performed and derived by Ryan[1]. The relationships brought forward are bounded in the Weber, W_e, number regime of $350<W_e<6{,}600$ and the Reynolds number, R_e, regime of $2{,}800<R_e<26{,}000$. The Weber number is the most restrictive of the two ranges since it relies upon the square of the injection velocity whereas the Reynolds number does not. For this reason Weber number was used to track the various operating configurations considered for validity of result. The characteristic length scale use in both calculations was the injector orifice diameter and the velocity used in each calculation was that of the propellant injected. Injector orifice dimensions were derived taking discharge coefficient impact into account. The flow velocities were derived from a chosen thrust level, specific impulse, ratio of propellant injected into the upstream reactor to downstream in the reactor gas stream, and the orifice dimension.

I_{sp}

Values for specific impulse were taken both from available literature and calculated for hydrazine and hydrogen peroxide. Specific impulse does vary with the thruster design operating condition of chamber pressure, thruster configuration detail of expansion ratio, operational environment of vacuum or atmospheric, and efficiency of the decomposition or combustion process, dependent upon the propellant combination used. The emphasis

of this study is on three particular chamber pressure ranges: 125, 250, and 500 psi. The literature data did not support accurate specific impulse data for this range, thus calculations were required to be made to ascertain an acceptable level of accuracy for inputs going into the calculation estimate of the chamber dimensions required. As previously discussed, the extent of ammonia dissociation in the decomposition of hydrazine has a dramatic impact on the specific impulse. Values for hydrazine specific impulse and associated chamber temperature as a function of the ammonia dissociation taken from Schmidt[2] were determined at a chamber pressure of 1,000 psi, values well above those in typical use today. The 125 to 500 psi range is more representative of typical state of the art operation design operating range. Decreased chamber pressure allows for a decreased weight thruster design and eases the burden of thruster material choices and manufacturing technologies, thus the motivation to examine the chosen pressure range. However, even across the chosen range of chamber pressures there is a variance in the specific impulse. To ease the complexity of calculations, specific impulse values were chosen that varied the least across this pressure range at a thruster configuration of 50:1 expansion ratio and vacuum environment. Accurate specific impulse values are of particular importance for this study as they drive the eventual flow rates of the propellant which in turn influences the atomization of propellants. In the instant study the specific impulse variance across the pressure range of interest is less than 3%. This variation is of minor enough that its influence on the overall end result is not considered to be of significance. Additionally of note, the specific impulse values were not adjusted for losses due to thermal characteristics of the intended thruster configuration, nozzle efficiency, or variances in catalytic reactivity. Sutton[11] provides

guidelines for estimating these types of losses, however, since the configuration of interest lends itself to heavyweight "workhorse" type engineering model hardware the applicability of these guidelines is less direct. Of particular difficulty to capture is the impact of the catalytic activity variance.

Discharge Coefficient

In the configuration of interest, where propellants are injected downstream, losses attributed to the injector orifice merit some consideration to ensure they are realistic and attainable. Relationships from Lefebvre[5] were used to evaluate discharge coefficients and were based upon the Reynolds number of the liquid propellant stream.

The range of discharge coefficients was calculated over the range of valid Reynolds number for the relations of Ryan[1] rather than on a case by case basis and a median discharge coefficient chosen for succeeding calculations. A median value of 0.77 for the range of 0.732 to 0.809 was used as its impact to orifice dimensions was approximately 2%. An impact of this magnitude is not considered to have significant effect upon the end result of this study.

Injector Orientation

The injector impingement half angle, θ, was arbitrarily chosen to be 40^{o}. This quantity impacts estimated impingement sheet velocity as well total chamber distance estimates since the "0" point or datum reference beginning of the chamber is defined as the injector orifice location. Increasing θ has the impact of decreasing sheet velocity, U_s, which increases the sheet break up length, r_b.

Impingement Sheet Dimension

The relationships brought forward from Ryan[1] allow for calculation of the impingement sheet radius at any angular displacement, ϕ, relative to a centerline emanating from the point of origin defined by the impingement point. See FIGURE 3 for further detail. ϕ was set equal to zero as the primary item of interest was the overall length of the liquid impingement sheet.

Droplet Formation, Size Distribution, and Decomposition

Atomization via impingement of liquid streams will produce a range of drop sizes, which is a function of the physical properties of the propellant, the velocities of the impinging streams, and the relative location from which they are shed form the resultant liquid sheet. A simplifying presumption of this study is that there will be one, homogeneous drop size that controls the distance required to achieve a liquid to gas change of state in the high temperature environment. Greater drop diameters result from decreased sheet velocities and it is expected that the drops that evolve from other than the zero degree ϕ displacement of the resultant impingement sheet will have sufficient distance to begin the liquid to gas transition that they will be of a lesser diameter than the drops evolved at the zero degree ϕ displacement at the edge of the sheet, thus not having an impact the overall chamber length required. Further, secondary atomization has been presumed to not be a factor in the median drop size to keep the complexity of this calculation within a realm where extensive computational resource is not required to arrive at a first estimate for the chamber length.

The decomposition process is considered to have been achieved with the transition of the propellant form the liquid phase to the gas phase. This simplifying assumption, like that of the secondary atomization, is applied to manage the complexity of the calculations to estimate the chamber length.

Vapor Phase Thermal Conductivity

The conditions of the ambient environment the evolved propellant drops are within control the rate at which the drops will transition from liquid phase to gas phase. Of particular relevance in the calculation of the droplet life, is the vapor phase thermal conductivity of this environment. In the instant study, this environment is composed of the reaction products of the liquid propellants, and has been reduced to the principal species. Though the number of species is few, the methodology to arrive at a thermal conductivity value is significantly complex. Saxena[6] and Mason[7] specify an approach for this type of estimation. In lieu of this approach, the gas phase thermal conductivities were combined via summing the reaction product species mol fraction contributions to the environment. However, upon review of the results, while the environmental thermal conductivity can have dramatic influence on the time to evaporation of the liquid drop, it is not the primary driver of the length estimate, thus any error introduced form this presumption is not considered to be of significant impact. The values calculated are consistent in magnitude with each of the discrete species.

Propellant vapor phase thermal conductivity for the propellants is also required to achieve the calculated estimates of this study. This particular quantity is not easily measured for hydrazine in the temperature regime required of the calculations, between the boiling

point and decomposition temperature. Schmidt[2] provides guidance with basis on how to achieve an estimate of the hydrazine vapor phase thermal conductivity in the absence of measured data in this temperature regime, use of a surrogate molecule that is also polar and of similar molecular weight. In this case, the use of Methanol, CH_3OH was suggested and utilized in this study. Data was available for this quantity for hydrogen peroxide in the temperature ranges of interest from Svehla[8] and thus used.

Section 2: Approach and Analysis

Discussion of References

Estimation of chamber length required for the configuration of interest taking the physical properties of the propellant into account for this study relied primarily upon the empirical work of Ryan[1]. Ryan's effort was focused upon the atomization characteristics of sheets formed from impinging jets as a function of flow and injector geometric properties. Within the instant study, values for the injector orifice and flow velocities were in family with those of the study. Ryan established a range of Weber and Reynolds number where the relationships of the study are considered most valid, which were adhered to for the instant study. The relationships taken from this reference work rely upon linear stability theory based upon the growth of infinitesimal disturbances due to aerodynamic stress on the resultant impingement sheet and can describe the disintegration of the sheet. Ultimately, relationships are utilized developed by works referenced by Ryan that also account for the physical properties of viscosity, surface tension, and density of the propellants and the environment they are being atomized

within. Within the summary and conclusions, the limitations of the approaches is acknowledged as questionable for predicting the sheet break up length for the conditions studied since it does not include the impact wave considerations, but reasonable for drop size prediction. Even so, Ryan's plots comparing actual to theoretical do reveal a trend of disagreement that allows for "rule of thumb" adjustment to the estimates achieved. The instant study did not apply "rule of thumb" adjustments, thus the estimated contribution to chamber length for impingement sheet break up will be greater than actual by a factor of as much as two. With this awareness of susceptibility, the relations can still provide helpful guidance in design of first iteration engineering model hardware.

Lefebvre[5] was drawn upon for teachings to most accurately relate the flow properties of the configuration of interest and the liquid propellant physical properties to estimate injection orifice dimensions.

Turns[9] contribution to the derived algorithm for estimating chamber length required based upon propellant physical properties relates to the time and distance required for the evolved droplets to transition from a liquid to gas phase.

Sutton[11], and Hill[12] were relied upon for standard equations relating various aspects of rocket engine performance to support derivation of liquid propellant flow rates and of chamber diameter and throat dimensions.

Schmidt[2], Brown[3], the ***Hydrogen Peroxide Handbook***[4], Svehla[8], and the ***CRC Handbook of Chemistry and Physics***[10], were principally relied upon for physical property information required for the estimate calculations. Turns[9] was also relied upon for a considerable amount of gas phase reaction product data.

Spalding[13], Anderson[14], Ibrahim[15], and Dombroski[16] were carried over as relevant citations from Hill[12] and Ryan[1] in regards to approaches to estimating overall chamber size, impingement sheet break up length and evolved drop sizes.

Analytical Process-Operating Conditional Cases Considered

Prior to embarking upon elaboration of the analytic approaches used to obtain required relationship values, a short discussion on the conditional cases considered and their reference notation is necessary. To obtain a keener picture of how propellant physical properties play a role in the overall dimensions required of a combustion chamber-the general conditions that will be studied must defined. In the instant study, three chamber pressures, three flow rate ratios, and two hardness ratios were evaluated. Defining non-standard terms, the term "flow rate ratio" refers to the ratio of mass flow rate of propellant going into the catalytic reactor, m'_{gg}, to that being injected and atomized downstream, m'_{inj}. The term "hardness ratio" refers to the ratio of the liquid propellant feed pressure, P_{feed}, to the combustion chamber pressure, P_c. As calculations are executed and carried through the various phases of operation within the configuration of interest, these differences in the overarching parameters are tracked in an indexed fashion as shown in TABLE 5, where the first digit indicates the chamber pressure selected, the second digit indicates the propellant flow rate ratio, and the third digit indicates the hardness ratio. This case index will be used in all succeeding plots comparing relative values.

Index	Pc (psi)	m' Ratio	hardness ratio
1.1.1	125	0.33	1.25
1.2.1	125	0.25	1.25
1.3.1	125	0.20	1.25
1.1.2	125	0.33	1.75
1.2.2	125	0.25	1.75
1.3.2	125	0.20	1.75
2.1.1	250	0.33	1.25
2.2.1	250	0.25	1.25
2.3.1	250	0.20	1.25
2.1.2	250	0.33	1.75
2.2.2	250	0.25	1.75
2.3.2	250	0.20	1.75
3.1.1	500	0.33	1.25
3.2.1	500	0.25	1.25
3.3.1	500	0.20	1.25
3.1.2	500	0.33	1.75
3.2.2	500	0.25	1.75
3.3.2	500	0.20	1.75

TABLE 5. Case Index of Overarching operational Parameters Considered

Analytical Process-Precursory Calculations

With the establishment of the operational cases and performance data that influence the combustion chamber dimensions, appropriate injector orifice dimensions must be derived. To estimate these, the relations set forth in Equations 1 and 2 were taken from Lefebvre[5].

$$[1] \qquad C_{Dmax} = 0.827 - 0.0085 \frac{l_o}{d_o}$$

$$[2] \qquad \frac{1}{C_D} = \frac{1}{C_{Dmax}} + \frac{20}{R_e}\left(1 + 2.25 \frac{l_o}{d_o}\right)$$

Where l_o is the orifice length, d_o the orifice diameter, and R_e the Reynolds number. These relations are put forward to provide an excellent fit to experimental data for $\frac{l_o}{d_o}$ ranges from 2 to 10 and R_e in the range from 10 to 20,000. Valid ranges for the relations from Ryan[1] are bounded by R_e between 2,800 and 26,000, however in the study values of R_e did not exceed 20,000. Ryan's relations were developed from empirical trials with $\frac{l_o}{d_o}$ of 375 to ensure laminar flow, but it is acknowledged that typical values are in the range of 3-10. FIGURE 9 shows the behavior of the estimated discharge coefficient with Re for typical orifice length to diameter ratios.

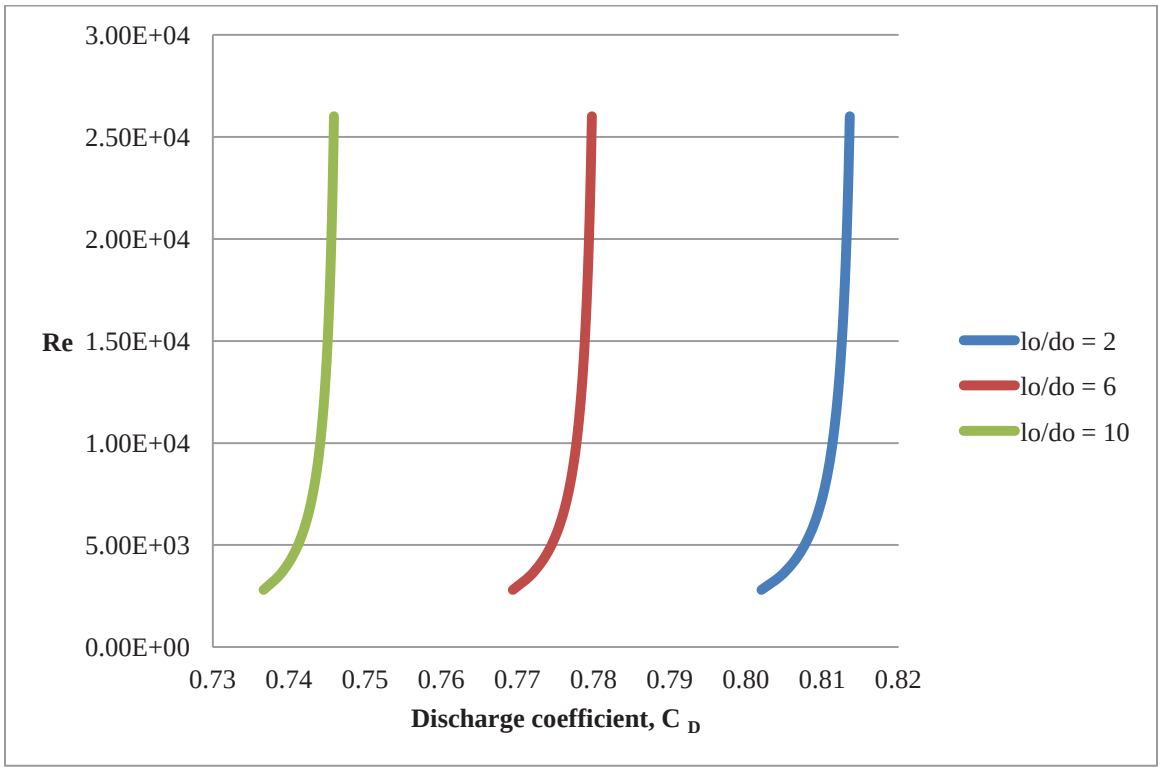

FIGURE 9. Discharge Coefficient as a function of Re for typical injector orifice length to diameter ratios

For this study, a discharge coefficient of 0.77 was chosen as it represents the median value within the valid range of R_e cited for the relationship of Equation 2.

With the establishment of the discharge coefficient, thrust level, propellant feed and combustion chamber pressures, and specific impulse the mass flow rates of propellants may be derived with the final objective of setting the injector orifice diameters. The straightforward relationship of thrust to specific impulse used is shown in Equation 3.

$$[3] \qquad m'_{total} = \frac{F_T}{I_{sp} g_o}$$

Where m'_{total} represents the total propellant mass flow rate required for the desired thrust level, F_T the desired thrust level, I_{sp} the specific impulse, and g_o the gravity constant. Recall, the combustion chamber configuration splits the total propellant flow between an initial gas generator device, taken to be a catalytic reactor, and propellant injected and atomized in the resultant flow downstream. The flow rate of propellant injected into the reactor will be denoted as m'_{gg} and the flow rate injected downstream as m'_{inj}. The m'_{inj} quantity is the subject of derivation of the injector orifice diameter, d_o. Ratios of m'_{gg} to m'_{inj}, as noted in TABLE 5 are 1:3, 1:4, and 1:5. Thus, the relation set forth in Equation 4 takes this ratio into account as well as the number of injector elements downstream to arrive at a flow rate per injector.

$$[4] \qquad m'_{inj} = \frac{m'_{total}\left(1 - \frac{m'_{gg}}{m'_{inj}}\right)}{\#\text{ of injectors}}$$

Equation 5 relates the injector orifice area, A_o, to the configuration parameters of ΔP, the difference between the chamber pressure, P_c, and the propellant feed pressure, P_{feed}; m'_{inj}; the discharge coefficient, C_D, and propellant density, ρ_L.

$$[5] \qquad A_o = \frac{m'_{inj}}{C_D\sqrt{2\rho\Delta P}}$$

Equation 6 then straightforwardly derives the injector orifice diameter, d_o.

$$[6] \qquad d_o = 2\sqrt{\frac{A_o}{\pi}}$$

The resulting values were in general magnitude agreement with those of Ryan's empirical trials, 0.30 to 0.512 mm. FIGURE 10 and 11 show the influence of the operational parameters and propellant properties on the injector orifice diameter.

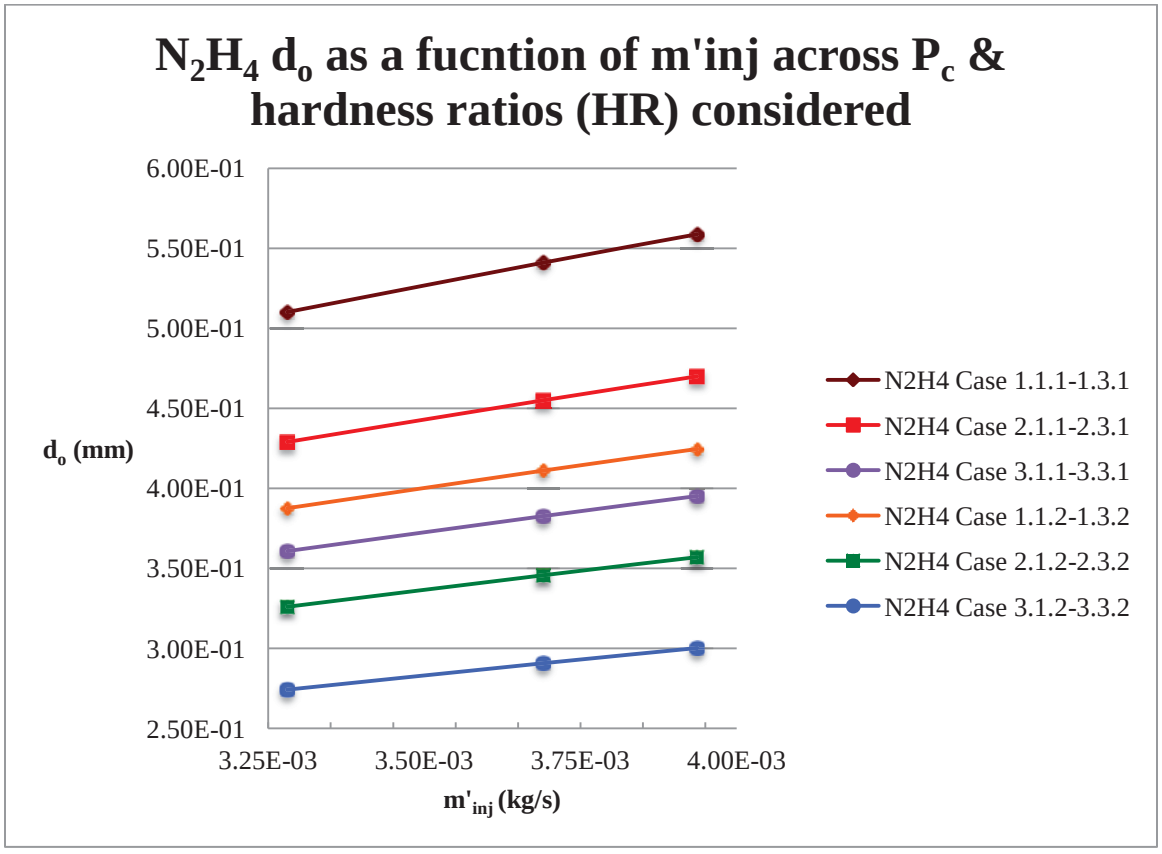

FIGURE 10. Injector Orifice Diameters for the Operational Range of Interest for Hydrazine

A clear trend that avails itself upon inspection of this plot is the relationship of chamber pressure and hardness ratio, denote as HR in the plot. As the chamber pressure increases and the hardness ratio increase, the injector diameter decreases. The chamber pressure

and hardness ratio drive the overall pressure drop, which as it increases will decrease the injector orifice area.

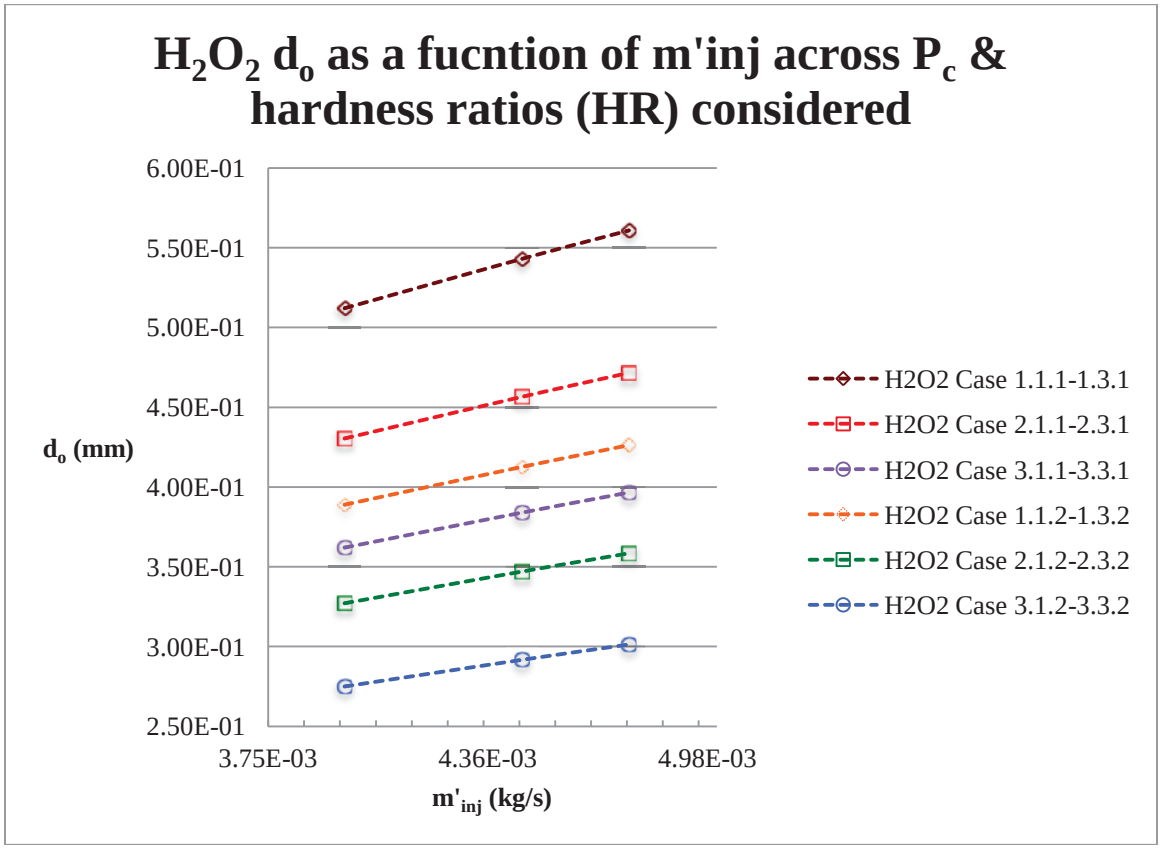

FIGURE 11. Injector Orifice Diameters for the Operational Range of Interest for Hydrogen Peroxide

The trends noted for FIGURE 10 also avail themselves in FIGURE 11. An additional take away, relating the physical properties of the propellant to influence on hardware dimensions, the combination of increased specific impulse and decreased density for hydrazine result in injector diameters only very slightly smaller than those for hydrogen peroxide, on the order 0.4%.

Before pressing further, a check of the resulting W_e and R_e was performed to ensure adherence to the stated validity ranges for the impingement sheet and droplet estimation

algorithms. Reviewing, W_e is the ratio of a fluids inertia to it's surface tension and is shown in Equation 7.

$$[7] \qquad W_e = \frac{\rho_L U_{inj}^2 d_o}{\sigma_L}$$

Where ρ_L is the propellant liquid density, U_{inj} is the propellant injection velocity, d_o the injector orifice diameter, and σ_L the liquid propellant surface tension.

Similarly, Re is the ratio of inertia force to viscous forces and is shown in Equation 8, where μ_L represents the dynamic viscosity coefficient.

$$[8] \qquad R_e = \frac{\rho_L U_{inj} d_o}{\mu_L}$$

The injection velocity is derived from the straight forward relationship with the mass flow rate, shown in Equation 9.

$$[9] \qquad U_{inj} = \frac{\dot{m}_{inj}}{\rho_L A_o}$$

FIGURE 12 and 13 show where the We and Re for the operational conditions applied to hydrazine. Figure 14 and 15 show the same for hydrogen peroxide.

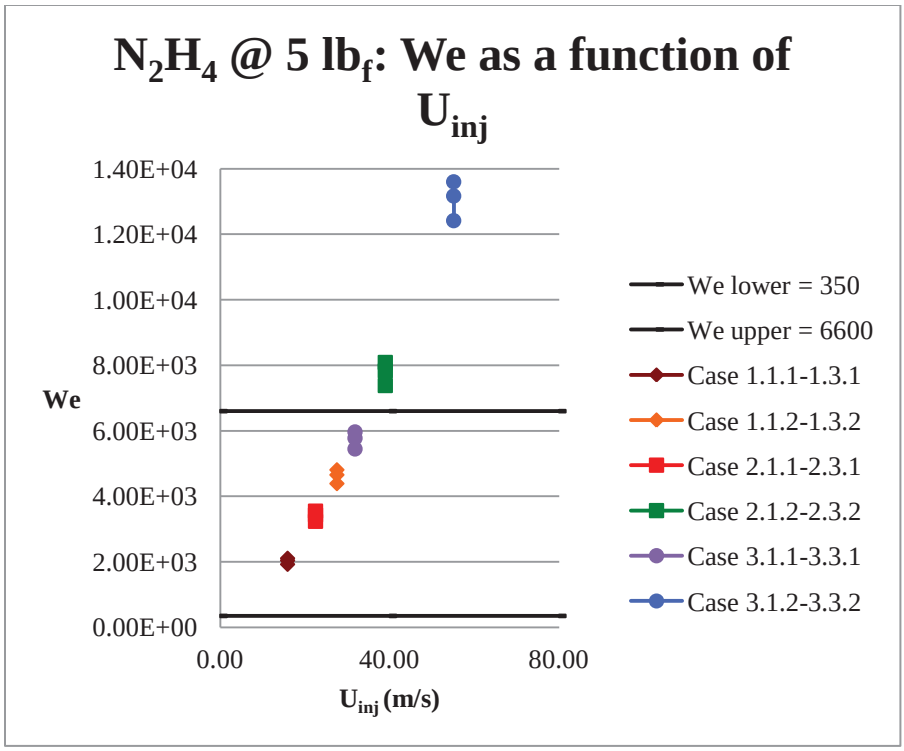

FIGURE 12. Resulting W_e as a function of the injection velocity with the upper and lower boundary values of Ryan for hydrazine

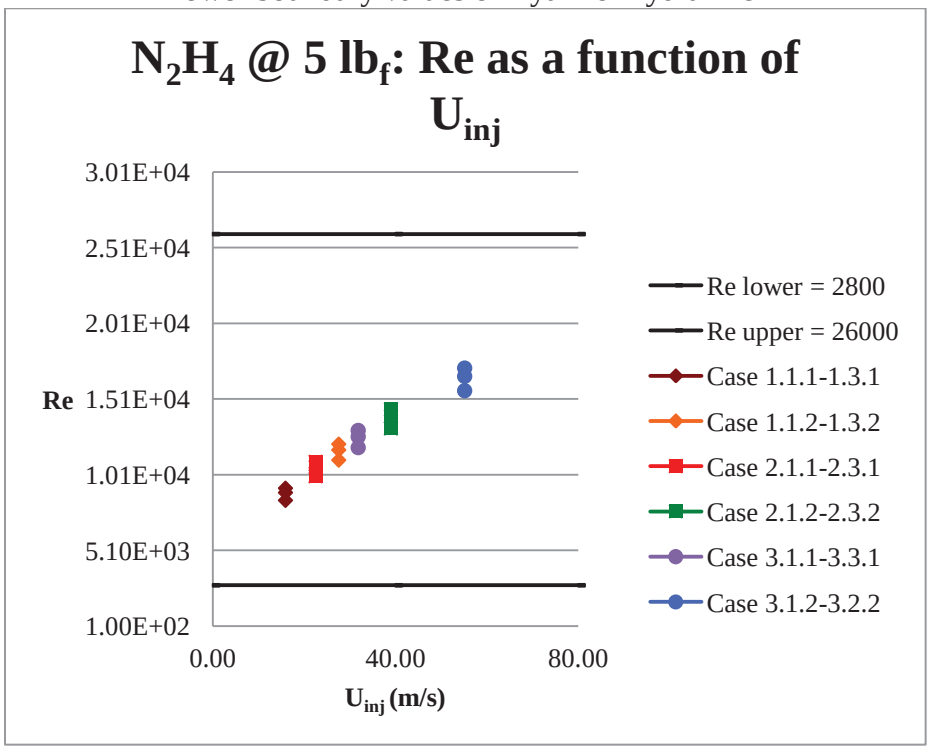

FIGURE 13. Resulting R_e as a function of the injection velocity with the upper and lower boundary values of Ryan for hydrazine

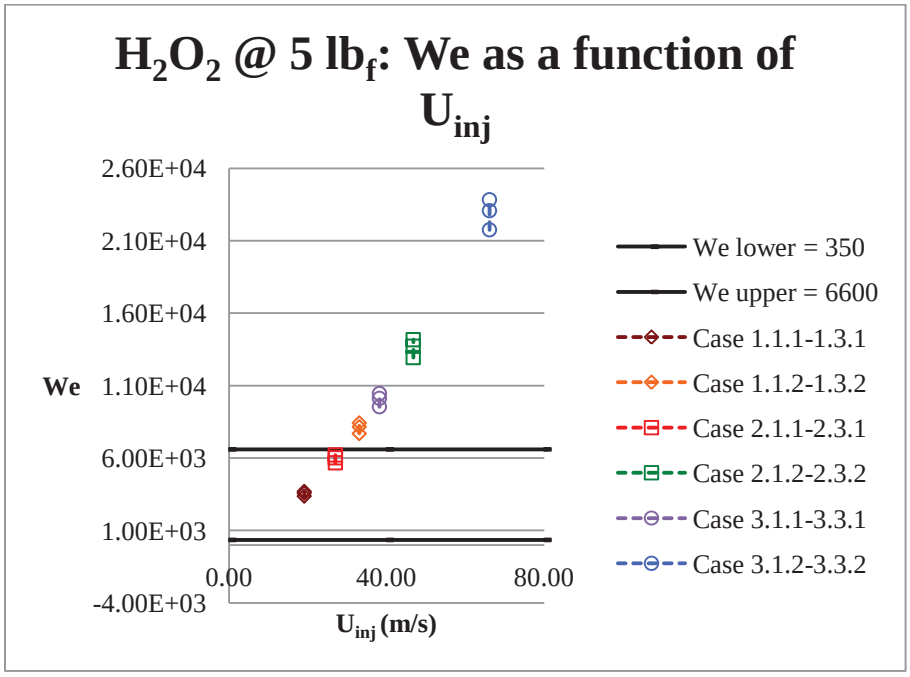

FIGURE 14. Resulting W_e as a function of the injection velocity with the upper and lower boundary values of Ryan for hydrogen peroxide

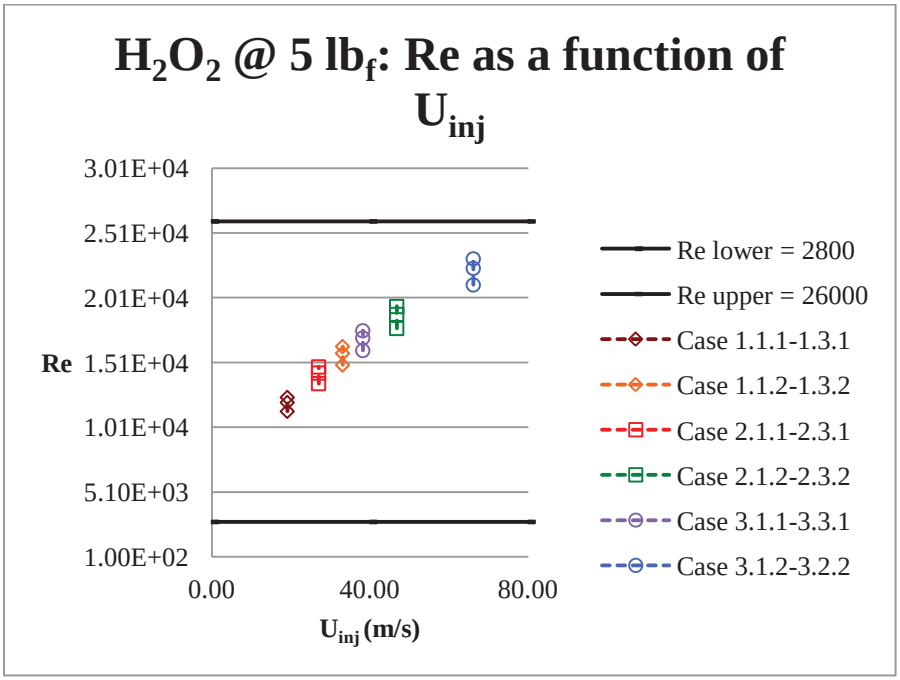

FIGURE 15. Resulting R_e as a function of the injection velocity with the upper and lower boundary values of Ryan for hydrogen peroxide

Upon inspection of these plots, it is clear that the W_e is the most restrictive condition, due to the square of the velocity term. Noting that there were no R_e out of range for the cases considered, W_e was used to guide valid cases. Also of note upon inspection of the trends, the increased density, viscosity, surface tension, and injection velocities of hydrogen peroxide relative to those of hydrazine drove fewer cases of hydrogen peroxide to pass this filter. In any given valid case, the values of W_e & R_e were significantly greater for hydrogen peroxide. Given that the specific impulse is a contributing factor, a conclusion cannot be ascertained straight forwardly as regards it's contribution versus the physical propellant properties. Variations of valid case injection velocities ranged from 18% to 20% comparing cases 1.1.1-1.3.1 and 2.1.1-2.3.1 relative to the lowest values from the hydrazine cases. Considering the differences in the ratios of density to surface tension, they are approximately 21%. Since the injection velocity is a square term, the actual difference in contribution is approximately 41%, thus it could be speculated the specific impulse is playing a greater role of impacting the ultimately derived combustion chamber dimensions.

Specific heat ratio (for chamber diameter)

The specific heat ratio, γ, is a function of the reaction products of the decomposed propellants and is required to make estimates of chamber and throat diameters. Both hydrazine and hydrogen peroxide contain endothermic process in their decomposition. For hydrazine, it is the dissociation of ammonia that drives the energetic performance and for peroxide, the water content. In this study, ammonia dissociation was assessed to be

complete, even though in commercial thrusters use design knowledge to maintain it below 50%[3]. When there is ammonia dissociation less than 100%, the reaction products for hydrazine will consist of ammonia, diatomic nitrogen, and diatomic hydrogen. Since full dissociation was presumed, there will only be diatomic nitrogen and hydrogen in the product stream. Thus, the calculated specific heat ratio becomes 1.375. Inclusion of the effect of ammonia dissociation will drive this value towards 1.2. Regarding hydrogen peroxide, 100% concentration (no water), was presumed. With this presumption, the reaction product assay includes water and diatomic oxygen, resulting in a calculated specific heat ratio of 1.243. Were the concentration of hydrogen peroxide decreased, the water content in the exhaust product would increase and also drive the specific heat ratio down. The specific heat ratio was derived via the relations in set forth in Equations 10-14.

$$[10] \quad \gamma = \frac{c_p}{c_v}$$

$$[11] \quad R_U = c_p - c_v$$

$$[12] \quad \gamma = \frac{\frac{c_p}{R_U}}{(\frac{c_p}{R_U} - 1)}$$

$$[13] \quad y_i = \frac{n_i}{n_T}$$

$$[14] \quad \gamma_{mix}(T) = \frac{\Sigma y_i \frac{c_{p(T)}}{R_U}}{\Sigma y_i \frac{c_{p(T)}}{R_U} - 1}$$

Where c_p is the specific heat at constant pressure, c_v is the specific heat at constant volume, R_U is the universal gas constant, y_i the mol fraction, n_i the mol contribution for a particular species of reaction product, n_T is the total mols of reaction product specie.

Chamber gas density

Chamber gas density (for impingement sheet dims..contrib to chamber length)

To evaluate the expressions from Ryan[1] and Turns[9] to achieve impingement sheet and drop size estimates the chamber conditions of gas density from the reactor and chamber gas density to liquid propellant density must be calculated. Chamber temperature, T_c, and Pressure, P_c, are known from the specific impulse, I_{sp}, calculations previously accomplished so the ideal gas law may be used to acquire the value for the chamber gas density, ρ_c. The relation is shown in Equation 15

$$[15] \qquad \rho_c = \frac{P_c}{R_{spec} T_c}$$

The liquid propellant density is a measured quantity that is recorded in several publications under standard conditions across temperature ranges where one would expect to be handling these materials. Standardized Material Safety Data Sheets (MSDS) will generally have this information. S, the ratio of the chamber gas density, ρ_c, to the propellant liquid density, ρ_L, is of particular relevance to the calculation of the resultant impingement sheet length as well as evolved droplet diameter. The relation is shown in Equation 16.

$$[16] \qquad S = \frac{\rho_c}{\rho_L}$$

The behavior of the ratio S as a function P_c is plotted in FIGURE 16 below for both hydrazine and hydrogen peroxide.

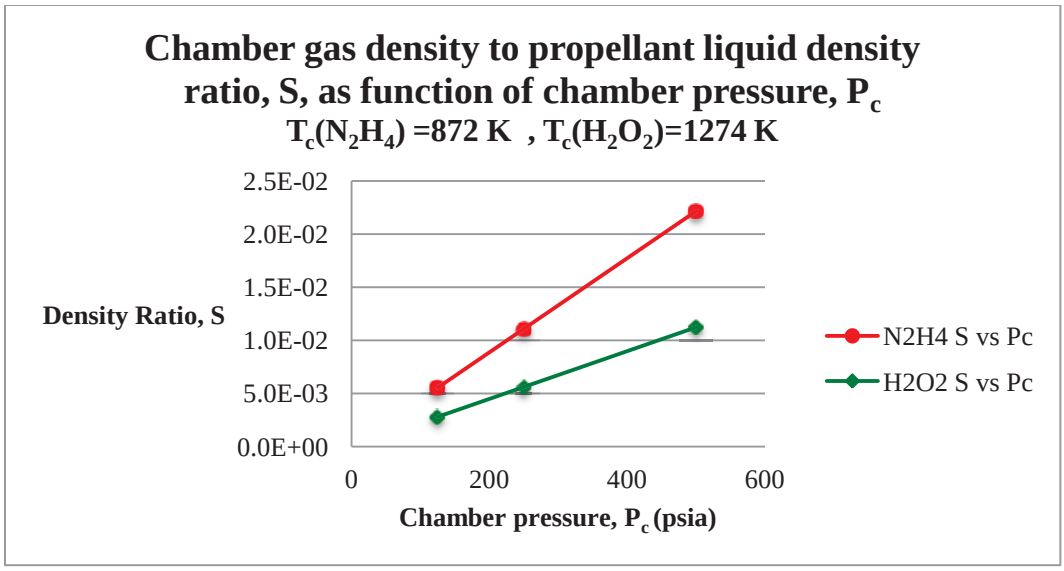

FIGURE 16. Ratio of chamber gas density to liquid propellant density as function of chamber pressure

An initial observation is that the line slope for S values of hydrazine are dramatically greater than for hydrogen peroxide at a given pressure. Principally driving this trend is the greater chamber temperature of the hydrogen peroxide reaction product environment. For hydrazine operating conditions where the ammonia dissociation is closer to 50%, the chamber temperature will approach the range for 100% concentration hydrogen peroxide and the density ratio difference will be less pronounced. Thus, it can be concluded that control of the endothermic process is critical to increasing delivered performance.

Wave number (for drop size)

Both wave number, k_m, and liquid sheet disturbance maximum growth rate factor, $\beta_{i,m}$, are necessary quantities to calculate the drop size evolved from the disintegrating liquid sheet resulting from the impingement of the two liquid propellant streams. Both expressions are taken from Ryan[1] and derived linear stability theory based upon the

perspective that aerodynamic stresses drive the liquid sheet to disintegrate into droplets. The relevance of the wave number is that it represents the growth rate coefficient for the unstable wave resulting from aerodynamic stresses. The relationships for the wave number are shown in Equations 17 and 18 and rely upon the ratio of the product of the chamber gas density and impingement sheet velocity to the surface tension.

$$[17] \quad k_m = \frac{\rho_c U_S^2}{2\sigma}$$

Where the sheet velocity, U_s, is defined as the product of the injection velocity, U_{inj}, and the cosine of the impingement half angle, θ.

$$[18] \quad U_s = U_{inj}\cos(\theta)$$

The impingement half angle in this study was not varied, but held at 40^o. An increase in the half angle decrease the sheet velocity and thus the sheet length would increase prior to disintegration into droplets.

Growth rate factor (for drop size)

The sheet maximum disturbance relationship captures the influence of all the physical properties of interest, viscosity, surface tension, and density to estimate drop size. The relation is shown in Equation 19.

$$[19] \quad \beta_{i,m} = \frac{\upsilon_L k_m^2}{2}\left(-1+\sqrt{1+\frac{8(\rho_c k_m U_S^2 - \sigma k_m^2}{\upsilon_L^2 k_m^4 \rho_L h}}\right)$$

Where ν_L is the kinematic viscosity, k is the wave number, and h is the liquid sheet derived thickness. The liquid propellant sheet thickness, h, is contingent upon determination of the centerline liquid sheet dimension, r_b, whose relation will be set forth

later. The determination of the sheet property r_b is necessary prior to calculating the maximum sheet disturbance growth rate.

Vapor phase thermal conductivity

Thermal conductivity of the gaseous environment must be accounted for to determine overall evolved droplet life. An overall evaporative constant, K, is derived from a combination of the environmental thermal conductivity, k_{inf}, which is driven by the reaction products, the un-decomposed propellant vapor phase thermal conductivity, k_F, and the Spalding number, B_q. The sum of these products at a median temperature between the chamber temperature, T_c, and the boiling point of the propellants, T_{boil}, is used and referred to as T_{bar}. The relationship for K and droplet evaporation was taken from Turns[9].

Focusing upon the environmental thermal conductivity, k_{inf}, this was arrived at extrapolating tabular, temperature based data from Svehla[8] and calculated using mol fractions of each species present, as denoted by Equation 20.

$$[20] \quad k_{inf}=\Sigma y_i k_i(T_{bar})$$

Where T_{bar} is defined by the relationship in Equation 21.

$$[21] \quad T_{bar}=\frac{(T_c+T_{boil})}{2}$$

The quantities for k_F were drawn from Schmidt[2], The Hydrogen Peroxide Handbook[4], and Svehla[8]. The overall environmental gas phase thermal conductivity, k_g, is provided with relationship provided by Turns[9], and combines k_F and k_{inf} as shown in Equation 22.

$$[22] \quad k_g=0.4k_F(@\ T_{bar})+ 0.6k_{inf}(@\ T_{bar})$$

Spalding number

The Spalding number, B_q, is the ratio of heat capacity as a function of the temperature difference between the environment and the propellant boiling point to the latent heat of vaporization and is indicative of a liquids propensity to change phase to vapor. The relationship for B_q is shown in Equation 23.

$$[23] \quad B_q = \frac{c_{pg}(T_c - T_{boil})}{h_{fg}}$$

Evaporation constant, K

Combining the results of equations 22 and 23, we have the relationship shown in Equation 24 for the evaporative constant, K, required to estimate droplet evaporation time.

$$[24] \quad K = \frac{8k_g}{\rho_L c_{pg}} \ln(B_q + 1)$$

Analytical Process-Chamber Dimensions

Chamber & Throat Diameter

Having established the precursory data characterizing the decomposition environment, isentropic flow relations as set forth by both Sutton[11] and Hill[12] that rely upon the specific heat ratio, γ, the total propellant mass flow, m'_T, chamber pressure, P_c, and temperature, T_c, and universal gas constant, R_u, can now be used to estimate initial chamber, $D_{chamber}$, and throat diameter, D*. Equation 25 defines the throat area, A*, from which D* is taken.

$$[25] \quad \frac{\dot{m}_T'}{A^*} = \frac{P_c}{\sqrt{R_{spec} T_c}} \sqrt{\gamma} \left(\frac{2}{\gamma+1}\right)^{\frac{\gamma+1}{2(\gamma-1)}}$$

With the throat area, A*, from the relationship in Equation 25, the chamber area, $A_{chamber}$, can be calculated with Equation 26.

$$[26] \quad \frac{A_{chamber}}{A^*} = \frac{1}{M}\left[\frac{2}{\gamma+1}\left(1+\frac{\gamma-1}{2}M^2\right)\right]^{\frac{\gamma+1}{2(\gamma-1)}}$$

A mach number, M, of 0.1 was chosen for these calculations since the flow velocity within the chamber is presumed to be very low prior to the converging portion of the chamber.

Impingement sheet length

The relationships from Ryan[1] for the impingement sheet length, r_b, and thickness, h are shown in Equations 27 and 28, respectively.

$$[27] \quad r_b = \frac{d_o}{2(14.2 S^{\frac{-2}{3}} W_e^{\frac{-1}{3}})}$$

$$[28] \quad h = \frac{d_o^2 \sin^3\theta}{4 r_b (1-\cos\phi\cos\theta)^2}$$

Drop diameter

The droplet diameter relationship taken from Ryan is set forth in Equation 29. Of note, Ryan substituted in a constant value for the disturbance growth rate integrated over the length of the resultant liquid impingement sheet, thus the relation used was modified to recapture this integration term.

$$[29] \quad \frac{d_D}{d_o} = \left[\frac{2.62}{\frac{\beta_{i,m}}{U_s} r_b}\right]^{\frac{1}{3}} S^{\frac{-1}{6}} [w_e f(\theta)]^{\frac{-1}{3}}$$

The function of the impingement half angle, f(θ), is defined in Equation 30.

$$[30] \quad f(\theta)=\frac{(1-\cos\theta)^2}{\sin^3\theta}$$

Drop evaporation distance

The relation taken from Turns to estimate the time to droplet evaporation, t_D, is deceivingly straight forward as shown in Equation 31. Recall, d_D and K have required all previous 30 equations to arrive at these numerical quantities.

$$[31] \quad t_D=\frac{d_D^2}{K}$$

From the evaporation time, the distance traveled, L_D,and thus required for droplet evaporation can be straightforwardly calculated with velocity equal to time over distance. The quantity for velocity used for this calculation is the sheet velocity, as it is presumed that the distance traveled by the drop with be short enough that it's velocity will be equivalent to that of the liquid sheet. The relation in terms of the instant nomenclature is shown in Equation 32.

$$[32] \quad L_D=\frac{t_D}{U_S}$$

Total chamber length

A final consideration in estimating the chamber length is to calculate the centerline distance, x_j, that will be required of the injection jet. This is a straightforward geometric calculation, as shown in Equation 33. An impingement half angle of 45^o was chosen for the evaluation.

$$[33] \quad x_j=D_{chamber}\frac{\cos\theta}{\sin\theta}$$

Summing each component that contributes, gives the final equation for the chamber length dimension, L_T, shown in Equation 34. It is the sum of the injector distance, x_j, the

impingement sheet length, r_b, and the distance required for the evolved drops to evaporate, L_D.

$$[34] \quad L_T = x_j + r_b + L_D$$

Section 3: Results and Discussion

Results

For the configuration cases considered throughout this study, the tangible results are presented graphically in FIGURES 17-24.

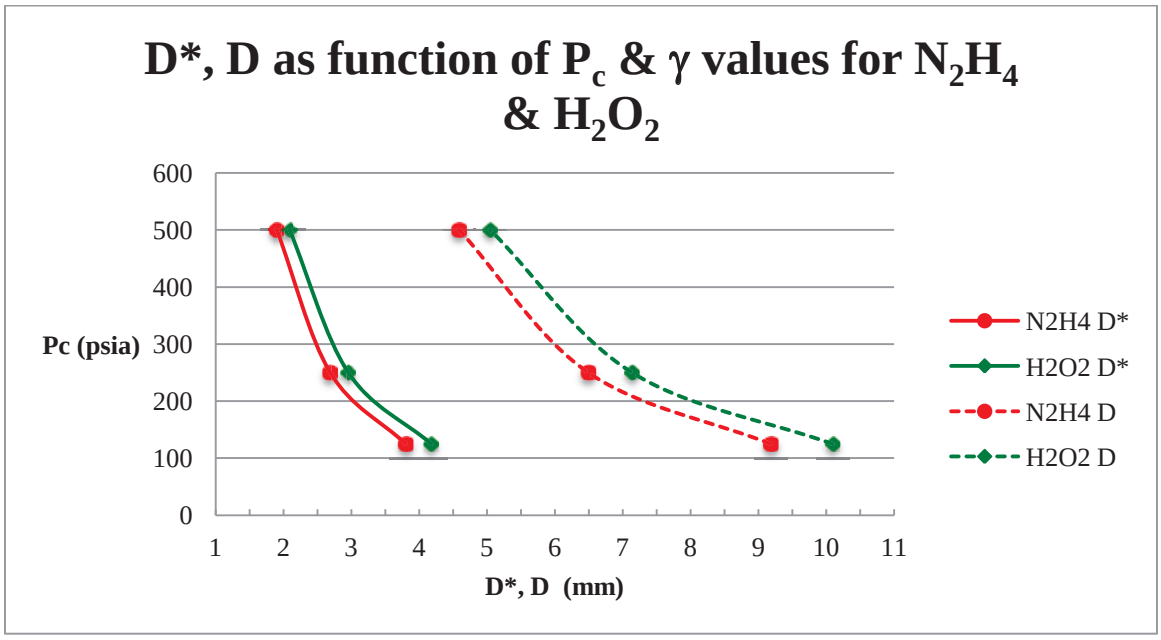

FIGURE 17. Combustion chamber and throat diameter as a function of the specific heat ratio and chamber pressure

Examining the plot of FIGURE 17, the higher value of the specific heat ratio clearly shows a slight, decreasing effect on the chamber diameter and throat dimensions. A more dramatic impact is made to these dimensions as the chamber pressure increases. Physically this is sensible since for a fixed thrust level, there is a fixed amount of gas

evolved which leaves only a decrease in overall volume as a means to increase the chamber pressure. Given this relationship, further evaluation would need to be made as regards to the ability of a smaller volume to achieve the same kind of combustion efficiency, or in the instant case, decomposition efficiency. Since the values for the hydrazine specific heat ratio were markedly impacted by the presumption of complete ammonia dissociation, a further conclusion that could be taken away from this plot is that mitigation of endothermic reactions will lead to increased dimensions.

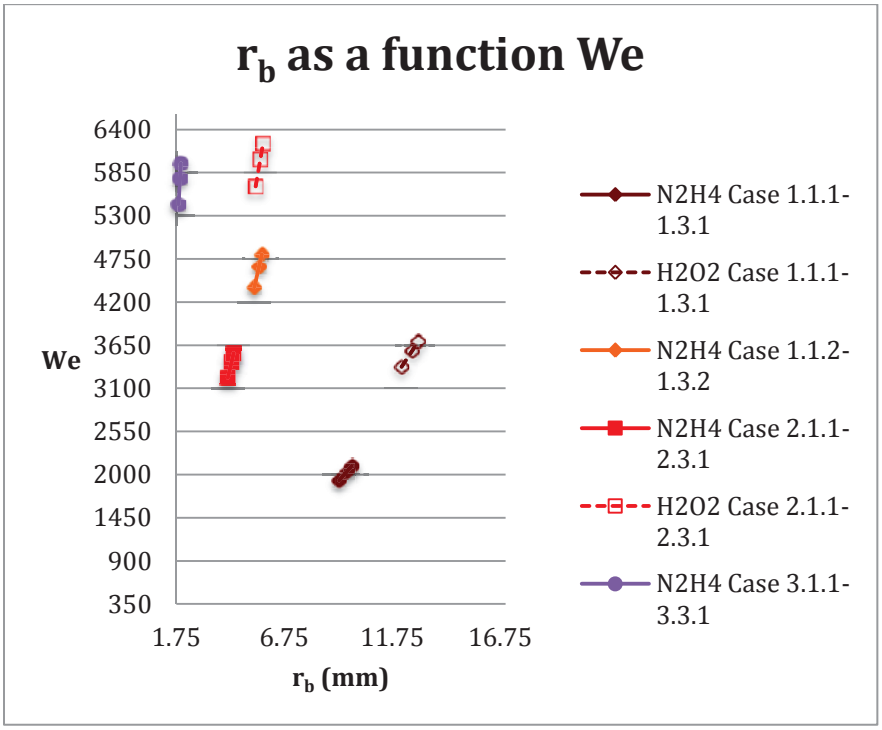

FIGURE 18. Impingement sheet length as a function of the Weber number.

Examining FIGURE 18, the Weber number ratio of inertia to surface tension plays a noticeable role in the length of the impingement sheet. As this ratio increases, the sheet length decreases indicating that as the inertia forces increase the distance required for aerodynamic disturbance to press the sheet to disintegrate into droplets falls. Since Weber captures injector orifice diameter and velocity terms, it carries a significant

amount of information. Contrasting hydrazine cases 1.1.1-1.3.1 and 1.1.2-1.3.2 (recall the third digit of the index indicates the hardness ratio), all else held equal an increase in the hardness ratio will decrease the impingement sheet break up length. The increased pressure drop at the increased hardness ratio decreases the overall injector orifice diameter which mandates the injection velocity increase. For both hydrazine and hydrogen peroxide, the Weber number increases with increasing chamber pressure and sheet break up length decreases. Contrasting hydrazine to hydrogen peroxide, the values calculated are in family of order of magnitude however the impact of hardness ratio cannot be evaluated of hydrogen peroxide as the resulting increase to injection velocity drove the W_e values out of the range of validity for the relationships taken from Ryan. The valid values for hydrogen peroxide are noticeably greater than for hydrazine under similar conditions, which is driven by the greater density and lower specific impulse (thus higher injection velocities required) of hydrogen peroxide.

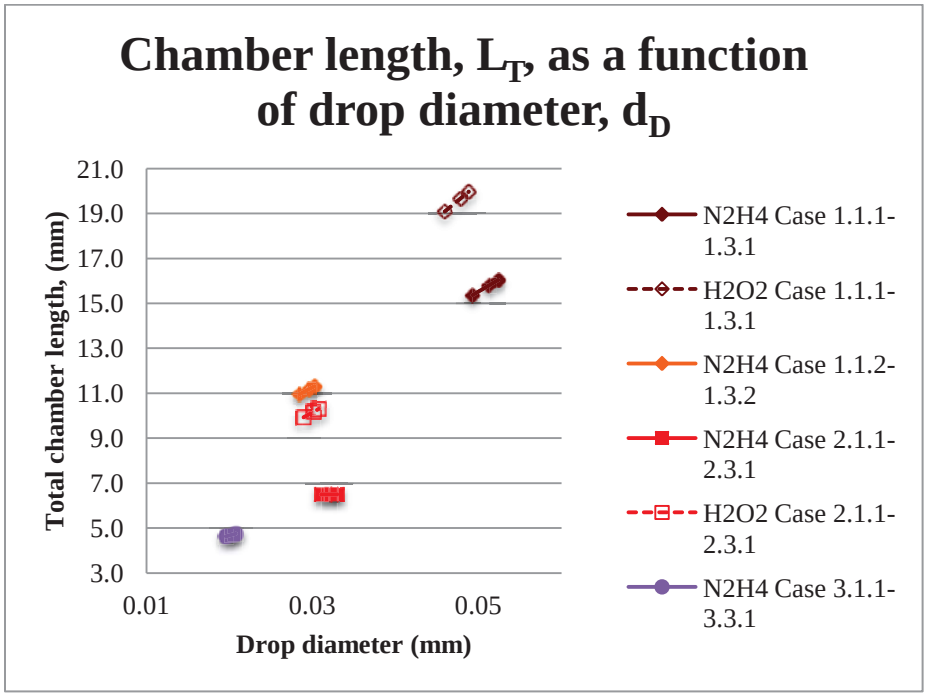

FIGURE 19. Total chamber length as function of the evolved drop diameter.

Evaluating the impact of evolved drop diameter on overall chamber length, this is of minor contribution. For a given condition, the drop size is very nearly the same for each set of conditions, the larger difference in impact seems to show itself in the time and distance for the drop to evaporate. Hydrogen peroxide drops require additional distance over that required of hydrazine, which presents an interesting play in the physical properties. Recall, the hydrazine free stream environment is cooler than that of hydrogen peroxide, thus it would seem it should be opposite. The distance contributed by hydrazine ranges from 0.17 to 0.69 millimeters where as for the equivalent hydrogen peroxide cases it ranges from 0.25 to 1.01 millimeter. Upon inspection of the tabular data, it would appear that the difference in the free stream thermal conductivity, k_{inf}, is driving this behavior. The k_{inf} value for hydrogen peroxide is 0.08 versus 0.22 W/(m-K) for hydrazine. Even with a much greater temperature difference in the hydrogen peroxide reaction product free stream relative to propellant boiling point, it is not sufficient to overcome the impact of the k_{inf} difference. Thus, a significant consideration for this aspect of chamber design is the reaction product vapor thermal conductivity.

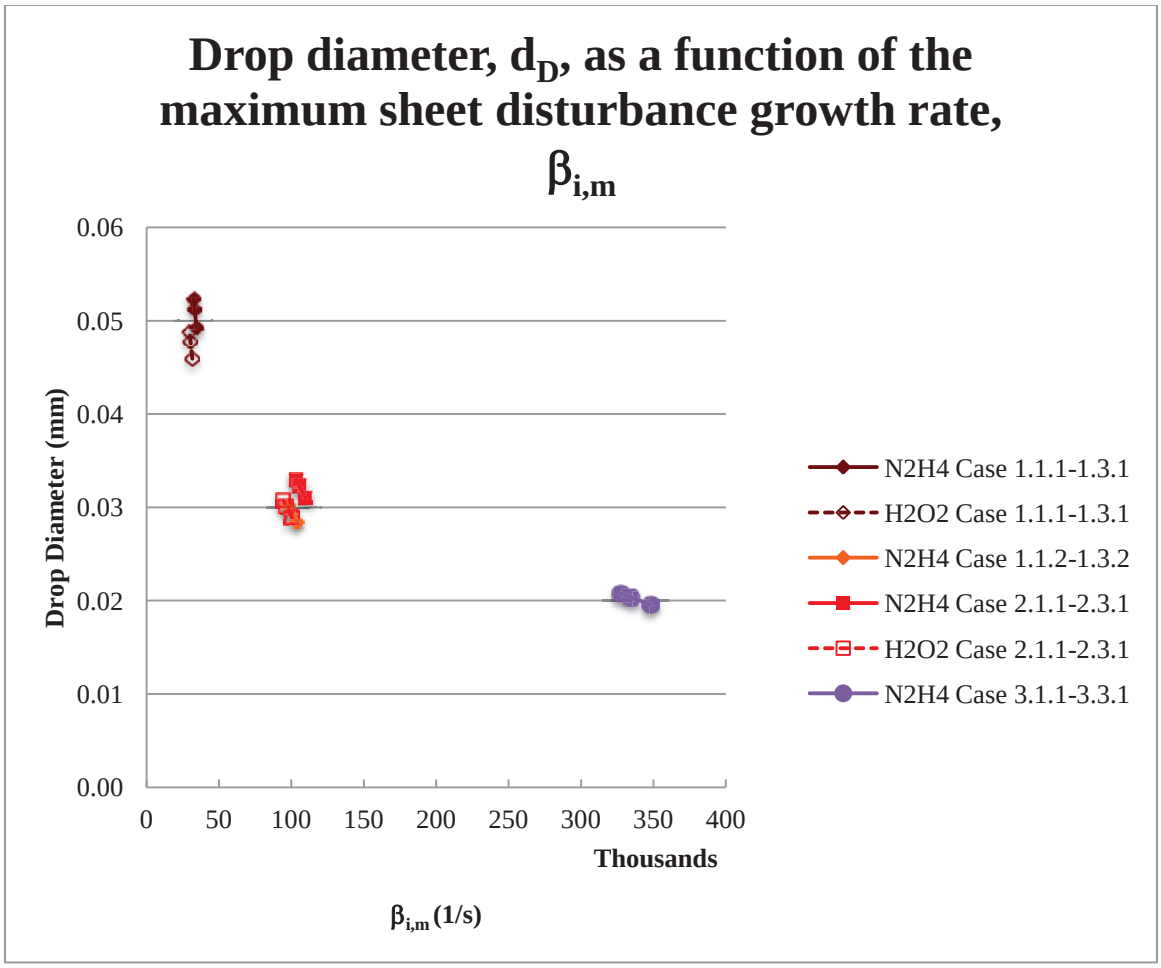

Figure 20. Drop diameter as a function of the disturbance growth rate for the impingement sheet.

The disturbance growth rate maximum, $\beta_{i,m}$, merits consideration since this term captures all of the propellant physical properties whose impact on chamber size is of interest. The quantities $\beta_{i,m}$, W_e, U_s, and θ drive the evolved drop size in Equation 29. Characterizing the impact of only $\beta_{i,m}$, it is observed that the variance in evolved drop size is small even with large differences in the physical properties. Because of the decreased specific impulse value of hydrogen peroxide relative to hydrazine, for a set thrust level the flow rates required increase and drive a nearly equivalent result for evolved drop size. Further evaluating the terms of Equation 29, it is noticed that even though the values of $\beta_{i,m}$, W_e,

U_s, and r_b change across the configurations considered, the quantity

$\int_0^{t_b} \beta_{i,m}\, dt = \frac{\beta_{i,m}}{U_s} r_b = 26.3$ for all cases, which becomes relevant when considering the instant study results relative to those achieved by Ryan comparing theoretical to empirical results.

Impingement sheet size is the greatest contributor to the estimated chamber size. Since impingement sheet length calculated estimates are driven by We, the values of density and surface tension are the physical quantities of interest. They are greater for hydrogen peroxide, and thus for similar conditions, the hydrogen peroxide chamber length values are greater than they are for hydrazine. Sheet velocity is a function of the injection velocity which is driven by the specific impulse and thus with a lower specific impulse for a given thrust level, a greater injection and corresponding sheet velocity results giving larger impingement sheet lengths. For similar conditions, the injection velocity for hydrogen peroxide is ~20% greater than for hydrazine. From a physical property perspective the density is ~45% greater, the surface tension ~20% greater, and the kinematic viscosity ~10% less for hydrogen peroxide relative to hydrazine. All of these factors combined drive impingement sheet lengths that are 20-30% greater for hydrogen peroxide and thus the greater chamber lengths required for similar operating conditions. In FIGURE 21 a comparison is made between Ryan's theoretical results and those achieved in the instant study to try and derive a useful "rule of thumb" correction factor. A comparative data plot from Ryan (figure 5 of the reference) is transposed with data from the instant study. Ryan's results are based on water, whose physical properties are nearly that of hydrazine and thus the similar relationship of hydrazine to hydrogen peroxide, and using a general simplification for the disturbance growth rate. The plots

from Ryan consider the ratio of sheet length and drop diameter to injector orifice diameter as a function of a scaling function. A straightforward trend that can be recognized is that as chamber pressure increases, the scaling function value increases. With increasing chamber pressure, injection velocities increase, which would drive an increase in the Weber number, and thus an increase in the scaling function, based on W_e and injection half angle, θ. Comparing similar cases, the physical properties and increased injection velocities of hydrogen peroxide are driving an expected trend of greater ratios and scaling factor values.

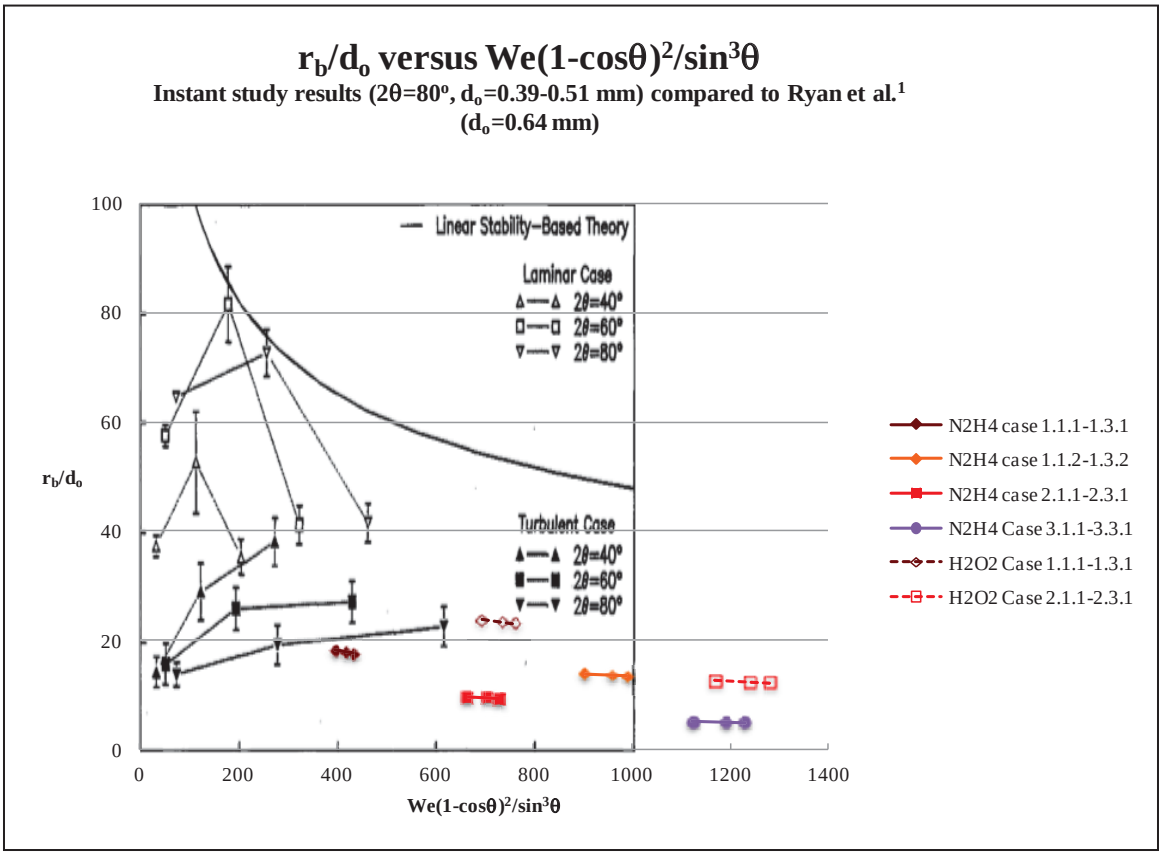

FIGURE 21. Comparison of instant study impingement sheet to injector orifice diameter dimension ratio to theoretical and empirical values with those of the instant study

In the case of the comparison for Ryan in FIGURE 21, the laminar flow values were closer in agreement with the linear stability theory than the turbulent values. For purpose

of the instant study, the turbulent flow case values are more relevant since those relate to injector length to diameter ratios most consistent with the instant study. The linear stability theory line of Ryan is derived by choosing the quantity $\int_0^{t_b} \beta_{i,m}\, dt=12$. In FIGURE 22, the values resulting from this substitution into the overarching equations to generate the sheet and droplet dimension ratios were also considered at the value of 64. Generating this quantities value with the physical properties of either hydrogen peroxide or hydrazine resulted in a value 26.3. In FIGURE 22, it can be seen as this value increases; the agreement of the linear stability theory with the empirical results improves. In either case, the values of the instant study achieve ratios that are consistently below the theoretical and empirical of Ryan but seem to show closer agreement with the empirical cases of turbulent flow.

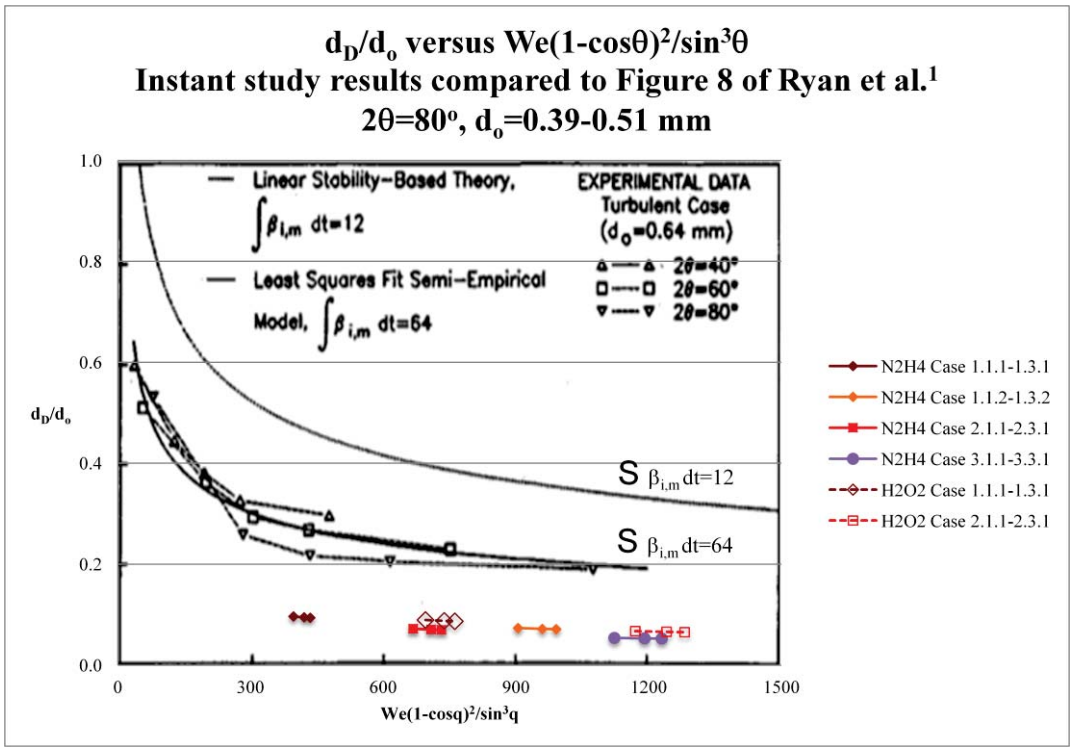

FIGURE 22. Comparison of instant study drop to injector orifice diameter dimension ratio to theoretical and empirical values with those of the instant study

Additional factors to consider that drive the disagreement are that smaller injector orifice diameters were derived in the instant study, thus if similar orifice diameters were used the corresponding Weber numbers would decrease due to lower injection velocities. Also of note, lower injection velocities result in greater drop diameters and impingement sheet lengths-thus, with the configuration parameter injector orifice diameter held constant, greater agreement would ensue from the instant study with the results of Ryan. However, returning to a "rule of thumb" correlation, in the case of the ratio of impingement sheet length to injector orifice diameter, there is approximately a factor of 3 difference with theoretical results of Ryan based upon inspection of FIGURE 21. Also of note in comparing the results of the instant study to those of Ryan's theoretical and empirical results, in Ryan as the scaling function increases, so does the ratio of sheet length to injector orifice diameter where as in the instant study this trend is reversed. Considering FIGURE 22, the correction factor appears to follow suit and be approximately 3 times the theoretical to match empirical.

Ultimately, the impact of all aspects must be considered on energy conversion hardware dimensions. Data from the instant study corresponding to chamber length, diameter, and throat diameter for hydrazine are plotted in FIGURE 23.

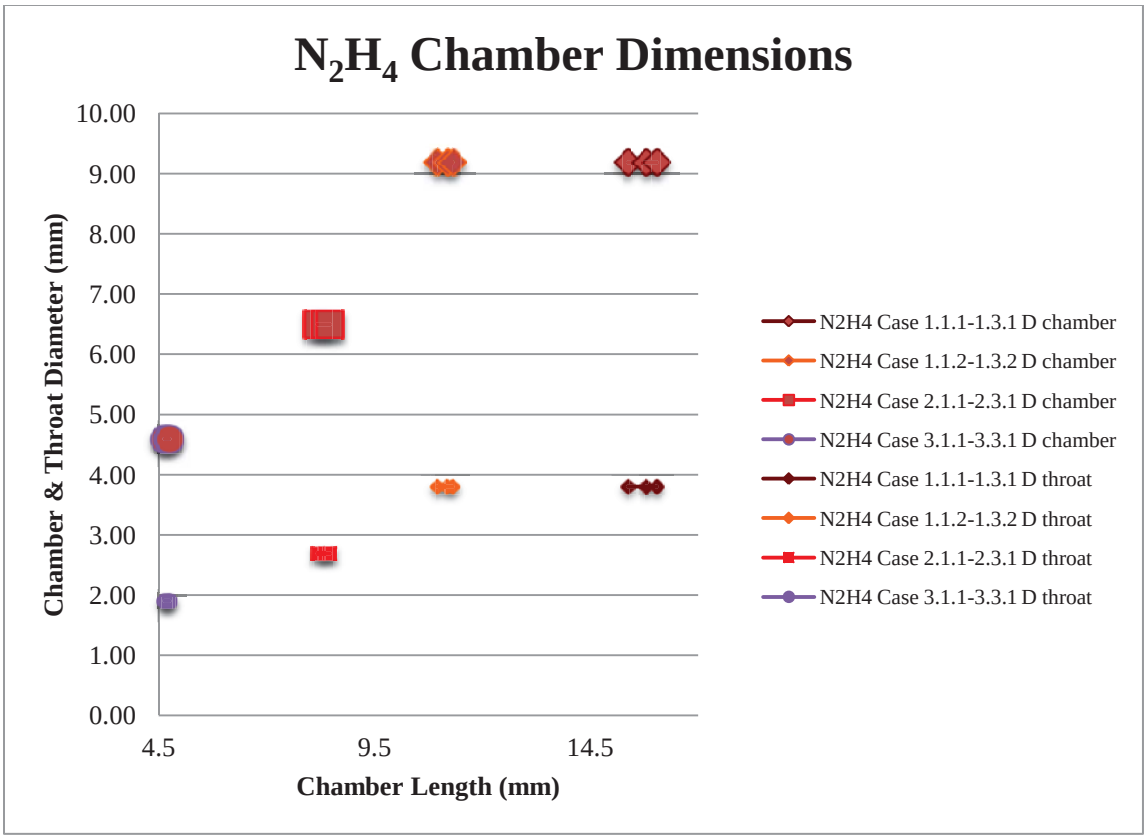

FIGURE 23. Hydrazine chamber dimensions as a function of chamber pressure, ratio of propellant flow into the reactor to downstream injection, and hardness ratio

The initial trend that is most pronounced is that the lowest chamber pressure results in the greatest dimensions, with the hardness ratio and propellant flow ratio having insignificant impacts. As stated previously, this is generally sensible since the amount of high temperature gas generated is going to remain constant for a set thrust value, and thus the dimensions should decrease with increasing chamber pressure. The effect of change in the propellant flow rate ratio over range of 1:3 to 1:5 is less than 5% and does not appear to be a significant consideration across the evaluated range. Hardness ratio does have a noteworthy impact, decreasing total chamber length by ~30%.

A similar plot for hydrogen peroxide in FIGURE 24, shows similar trends. There are fewer data points since the sensitivity of the Weber number constraint eliminated valid

cases for the conditions considered. A similar conclusion of the impact of propellant flow ratio shows itself, having less than a 5% impact to overall chamber length. Chamber pressure, as before has a significant impact, on the order of a 30% decrease in chamber length when doubled.

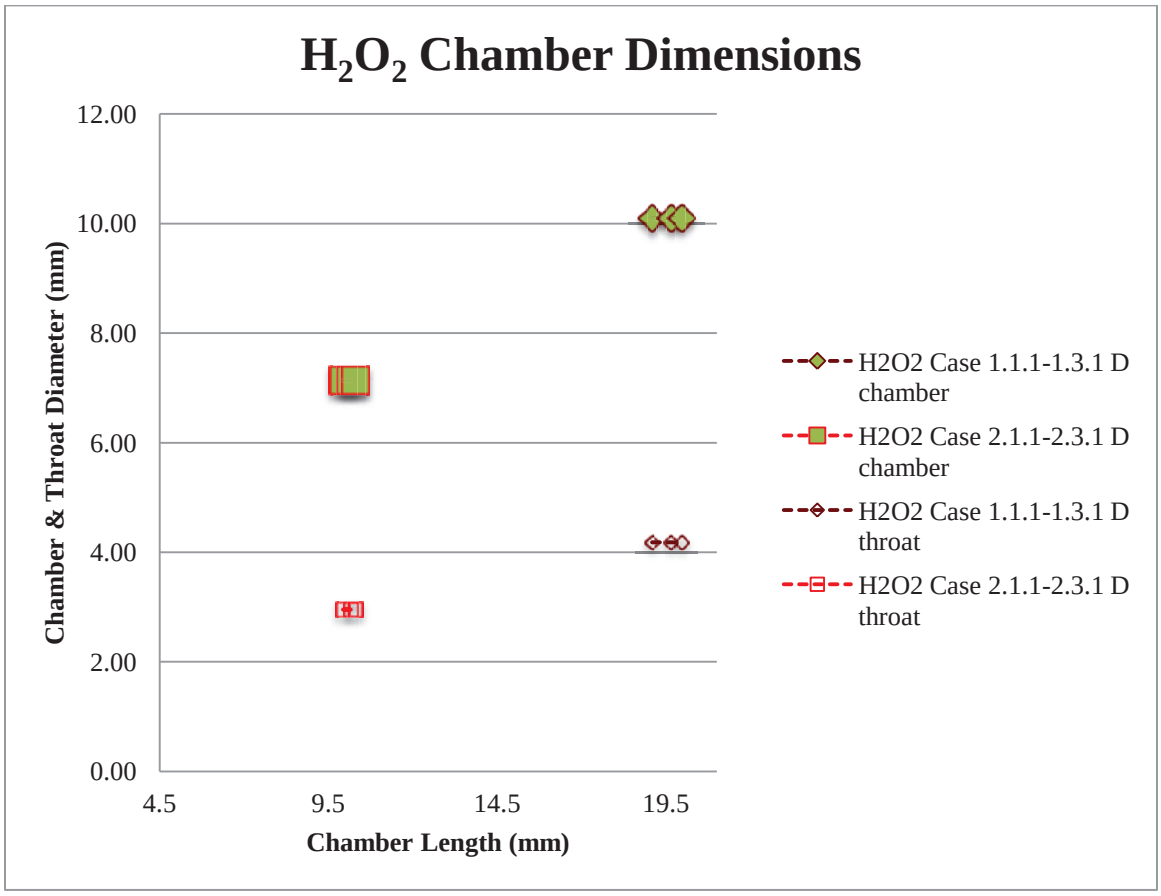

FIGURE 24. Hydrazine chamber dimensions as a function of chamber pressure, ratio of propellant flow into the reactor to downstream injection, and hardness ratio

In FIGURE 25, data for both propellants was plotted to infer impact of physical property differences. This makes for a very course comparison, certainly, however, under equivalent conditions hydrogen peroxide will require greater chamber dimensions than hydrazine.

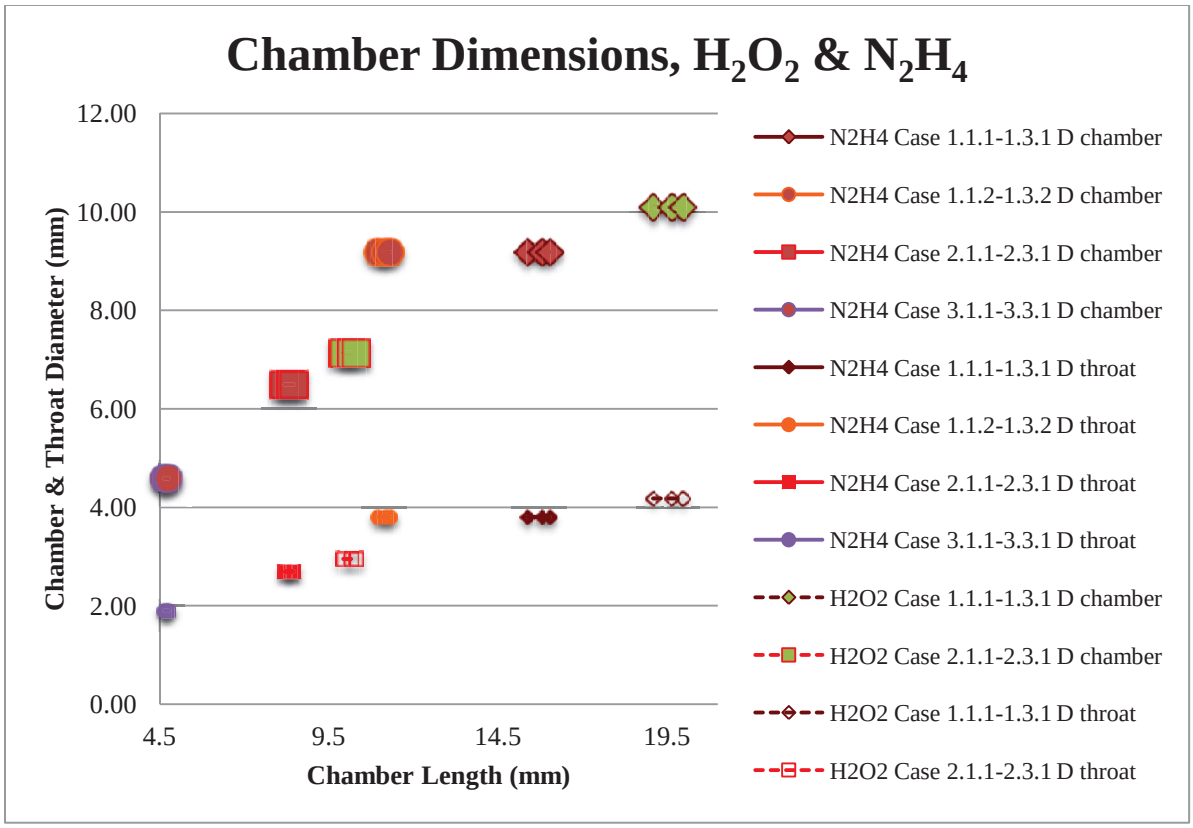

FIGURE 25. Hydrazine & hydrogen peroxide chamber dimensions as a function of chamber pressure, ratio of propellant flow into the reactor to downstream injection, and hardness ratio

Considering the earlier conclusions from FIGURE 18, 19 , and 20 the driver in the chamber dimension length differences coincides with the difference the injection velocities required due to lower specific impulse for hydrogen peroxide. The increased injection velocity results in a greater impingement sheet length, the largest impact given the constraints and presumptions of this study to the length dimension. The larger velocities required for hydrogen peroxide in combination with it's larger density and surface tension values resulted in drop sizes that were very nearly equal, however, the time required for the evolved drops of hydrogen peroxide was greater due to a less heat conductive free stream environment.

Trends

Gathering trend observations from examination of FIGUREs 17-24 some general conclusions can be formed in regards to the factors that influence chamber dimensions. Increasing values of specific heat ratio, which is driven by endothermic process, decreases the chamber dimensions. The magnitude of result will be unique for a given propellant formulation. Another factor to consider that drives this dimension is the mass flow rate and decomposition or combustion temperature, for the chamber dimensions will be increased as these increase. The impingement sheet length decreases with hardness ratio and increases with Weber number, which in turn was seen to increase with chamber pressure. Chamber free stream thermal conductivity has impact on the amount of time required to drive a liquid drop to vapor, thus the greater vapor phase thermal conductivity of the environment, the shorted this time and corresponding distance required, will be. Impingement sheet disturbance growth rate increases with chamber pressure and drives the evolved drop size to decrease. Chamber pressure and hardness ratio increases will drive a decreased chamber dimensions overall.

Comparative Error Contributions

Comparisons with Ryan were difficult to make since those plots were held at a constant injector orifice diameter, which in all cases was greater than those used in the instant study. In Ryan, the values of empirical were below those of theoretical, whereas in the instant study the values of theoretical fell below those of Ryan's empirical. It is acknowledged that as the injector orifice is increased, the propellant mass flow rates

would have decreased and reduced the value of the scaling function. In regards to the ratios of interest, reduced propellant velocity leads to an increased impingement sheet lengths and drop sizes evolved. Considering these impacts, a larger injector orifice diameter is conjectured to push the instant study theoretical results closer to empirical.

Section 4: Summary and Conclusions

Overarching Effort Summary

The instant study sought to determine how a propellant's physical properties would influence an energy conversion device's dimensions. In the energy conversion device of interest, in effect a two stage rocket thruster, what was clearly shown is that energy content of the propellant of interest plays a dramatic role in addition to it's physical properties. First, the relevant factors of the environment had to be calculated such as the specific heat ratio and the vapor phase thermal conductivity values. With the environment that the propellants will be injected and atomized into defined, then the quantities relevant to each phase leading to atomization were calculated, and then the impact of droplet evolution to vapor phase was determined. Three different chamber pressures, three different propellant injection ratios, and two different hardness ratios were considered for two different propellants. Increasing chamber pressure and hardness ratio reduced the overall chamber dimension determined. The impact of the difference in the physical properties was not straightforward to observe in the results due to the difference in mass flow rates. The 20% difference in specific impulse between hydrazine and hydrogen peroxide resulted in the same difference in injection velocity, and about the same in resulting chamber length. Given the results of this study, the most general read

of the data tells us that for every percent less of specific impulse form a baseline, there will be a corresponding increase for the chamber length required. As regards the chamber and throat diameters, for every two percent difference in specific impulse, there seems to be a one percent increase in these dimensions.

Impact of Operating Parameters versus Propellant Properties

The Weber number is the most pervasive quantity that accounts for the physical property differences throughout the relations used. Examining the components of this ratio, it is noted that the ratio of liquid density to liquid surface tension is roughly 20%, the ratio for hydrogen peroxide being the greater. Likewise, the injection velocity for hydrogen peroxide is roughly 20% greater than for hydrazine (~40% comparing their squares). The injector orifice diameters are roughly equivalent. These differences combined drive a 75% greater We for hydrogen peroxide than hydrazine. From this, generally speaking, it can be seen the specific impulse has the most impact since it drives the mass flow rate of propellant, from which the injection velocities are derived. Thus, the differences of physical properties such as liquid density, viscosity, and surface tension are less influential than the energy content of the propellant.

Future Work

Several aspects of the instant study could be improved to enhance accuracy of results in future work. The most prevalent comes from the primary reference, Ryan, in that the model of impinging jet atomization should include impact wave considerations, rather than just break up due to aerodynamic forces. Properly accounting for endothermic

process in the reactions will also allow for greater resolution, as this has effects not only the resulting free stream environment but also the specific heat ratio, both of which ultimately drive chamber dimensions. Inclusion of an atomization model that would consider secondary atomization process would also increase resolution in determining a mean drop size. Finally, there is no substitute for empirical data to evaluate a model's ability to predict the physical process taking place in a given system.

References

1. Ryan, H.M., Anderson, W.E., Pal, S., & Santoro, R.J. (1995). ***Atomization Characteristics of Impinging Liquid Jets***. Journal of Propulsion and Power, Vol. 11, No. 1, January – February 1995.

2. Schmidt ***Hydrazine and Its Derivatives, Second Edition.*** ISBN 0-471-41553-7.

3. Brown, Charles D. ***Elements of Spacecraft Design.*** AIAA, Reston, VA. 2002. Pg. 181. ISBN 1-56347-524-3.

4. AFRPL-TR-67-144 ***Hydrogen Peroxide Handbook,*** July 1967. Pages 70, 417.

5. Lefebvre, A.H. ***Atomization & Sprays***. United States of America: Taylor & Francis. 1989. ISBN 0-89116-603-3.

6. Saxena, S.C. ***Transport Propeties of Gases and Gaseous Mixtures at High Temperatures.*** Department of Energy Engineering, Univesity of Illinois at Chicago Circle, Chicago, Illinois. December 9, 1970.

7. Mason, E.A., Saxena, S.C. ***Approximate Formula for the Thermal Conductivity of Gas Mixtures,*** Phys. Fluids 1, 361 (1958).

8. Svehla, Roger A. ***NASA Technical Report R-132, Estimated Viscosities and Thermal Conductivities of Gases at High Temperatures.*** 1962.

9. Turns, Stephen R. ***An Introduction to Combustion, Concepts and Applications, Second Edition.*** McGraw-Hill. 2000. ISBN 0-07-230096-5.

10. ***CRC Handbook of Chemistry and Physics, 86th Edition 2005-2006***.

11. Sutton, G.P. & Biblarz, O. ***Rocket Propulsion Elements, Seventh Edition***. New York: John Wiley & Sons, Inc. 2001. ISBN 0-471-32642-9.

12. Hill, P.G., Peterson, C.R. ***Mechanics and Thermodynamics of Propulsion, Second Edition***. Reading, MA: Addison Wesley Publishing Company. 1992. ISBN 0-201-14659-2.

13. Spalding, D.B. ***Combustion in Liquid-Fuel Rocket Motors,*** Aero. Quarterly 10, (1959): 1-27.

14. Anderson, W.E., Ryan, H.M., & Santoro, R.J. (1995). ***Impinging Jet Injector Atomization***. Progress in Aeronautics and Astronautics, Vol. 169, pp. 215-246.

15. Ibrahim, E.A. & Prezkwas, A.J. (1991***). Impinging Jets Atomization***. Physics of Fluids, A, Vol. 3, No. 12, December 1991.

16. Dombrowski, N. & Hooper, P.C. (1963). ***A study of the sprays formed by impinging jets in a laminar and turbulent flow***. Journal of Fluid Mechanics, Vol. 18, Pt. 3, September 1963. pp. 392-400.

Appendices

Nomenclature

Notation	Definition
a	Curve fit polynomial constant
A	Chamber cross-sectional area
A*	Throat cross-sectional area
A_o	Injector orifice cross-sectional area
B_q	Spalding or transfer number, based on heat transfer considerations only
c_{pg}	Specific heat at constant pressure of gas phase
C_D	Discharge coefficient
C_{Dmax}	Discharge coefficient value attained at Re > 10,000
CH_3OH	Methonal
c_p	Specific heat at constant pressure
c_v	Specific heat at constant volume
$D_{chamber}$	Chamber diameter
D*	Throat diameter
d_D	Droplet diameter
d_o	Injector orifice diameter
d_{jet}	Impinging liquid propellant jet diameter
F_T	Thrust force
g_o	Gravity
h	Liquid propellant sheet thickness
H	Hydrogen, monatomic

Notation	Definition
H_2	Hydrogen, diatomic
H_2O	Water
H_2O_2	Hydrogen Peroxide
h_{fg}	Latent heat of vaporization
Isp	Specific impulse
K	Evaporation constant
k_F	Propellant gas phase thermal conductivity
k_g	Environment gas phase thermal conductivity
k_m	Wave number for the most unstable wave
k_{inf}	Gas generator combustion product gas phase thermal conductivity
L_D	Distance traveled by droplet until fully evaporated
L_T	Total chamber distance required for injection, atomization and evaporation of liquid propellant
M	Mach number
m’	Mass flow rate of liquid propellant
MeOH	Methonal
m'_{gg}	Gas generator mass flow rate of liquid propellant
m'_{gg}/m'_{inj}	Ratio of mass flow rate of liquid propellant injected through the gas generator to the that injected downstream
m'_{inj}	Injected mass flow rate of injected liquid propellant
m'_T	Total mass flow rate of liquid propellants injected into the thruster, derived from specific impulse and thrust requirement.
MSDS	Material Safety Data sheet
MW	Molecular weight
N	Nitrogen, monatomic

Notation	Definition
N_2	Nitrogen, diatomic
N_2H_4	Hydrazine
n_i	Mol fraction for a particular species
n_T	Total mols of all species in a reaction
O	Oxygen, monatomic
O_2	Oxygen, diatomic
P_c	Chamber pressure
P_f	Feed pressure
$P_{f/c}$	Ratio of feed to chamber pressure, other wise referred to as “hardness” ratio
r_b	Radial distance from impingement point where liquid sheet break up into ligaments occurs
R, R_u	Universal gas constant
R_{spec}	Universal gas constant divided by the MW of the gas of interest
R_e	Reynolds number, ratio of inertial forces to viscous forces
S	Ratio of chamber gas density to liquid propellant density
SL	Sea Level
T	Temperature
T_{bar}	Average temperature of the free stream environment and the liquid propellant boiling point
T_{boil}	Boiling point temperature of liquid propellants
T_c	Chamber (combustion product) temperature
T_{inf}	Free stream environment temperature
$\Delta T_{inf\text{-}boil}$	The difference between the free stream environment temperature and the liquid propellant boiling point

Notation	Definition
U_{inj}, U_j	Injected liquid propellant jet velocity
U_s	Velocity of liquid in sheet resulting from impingement of injected liquid jets
Vac	Vacuum
W_e	Weber number, ratio of inertia to surface tension
X	Percentage of ammonia dissociation in hydrazine decomposition reaction
x_j	Horizontal length component of liquid jet within chamber
y_i	Molar mass fraction,
$\beta_{i,m}$	Liquid sheet disturbance maximum growth rate
γ	Specific heat ratio
γ_{mix}	Specific heat ratio for a particular molecule
μ_L	Dynamic viscosity coefficient
ν_L	Kinematic viscosity coefficient
ϕ	Angle relative to centerline of the liquid sheet formed from impingement of liquid propellant jets
ρ_L	Liquid propellant density
ρ_g	Gas phase density
σ_L	Surface tension
θ	Impingement half angle